

1 **Spatial and seasonal variability in volatile organic sulfur**
2 **compounds in seawater and the overlying atmosphere of the**
3 **Bohai and Yellow Seas**

4 **Juan Yu^{1,2,3,†}, Lei Yu^{1,†}, Zhen He^{1,2,3}, Gui-Peng Yang^{1,2,3,*}, Jing-Guang Lai¹, Qian Liu¹**

5 ¹Frontiers Science Center for Deep Ocean Multispheres and Earth System, Key Laboratory of Marine Chemistry
6 Theory and Technology, Ministry of Education, Ocean University of China, Qingdao 266100, China.

7 ²Laboratory for Marine Ecology and Environmental Science, Qingdao National Laboratory for Marine Science and
8 Technology, Qingdao 266237, China.

9 ³Institute of Marine Chemistry, Ocean University of China, Qingdao 266100, China.

10
11 **Abstract.** Volatile organic sulfur compounds (VSCs), including carbon disulfide (CS₂), dimethyl sulfide (DMS), and
12 carbonyl sulfide (COS), were surveyed in the seawater of the Bohai and Yellow Seas and the overlying atmosphere
13 during spring and summer of 2018 to understand the production and loss of VSCs and their influence factors. The
14 concentration ranges of COS, DMS, and CS₂ in the surface seawater were 0.14–0.42, 0.41–7.74, and 0.01–0.18 nmol
15 L⁻¹ during spring and 0.32–0.61, 1.31–18.12, and 0.01–0.65 nmol L⁻¹ during summer, respectively. The COS
16 concentrations exhibited positive correlation with dissolved organic carbon (DOC) concentrations in seawater during
17 summer, which verified the photochemical production of COS from chromophoric dissolved organic matter (CDOM).
18 High DMS concentrations occurred near the Yellow River, Laizhou Bay, and Yangtze River Estuary, coinciding with
19 high nitrate and Chl *a* concentrations due to river discharge during summer. The COS, DMS, and CS₂ concentrations
20 were the highest in the surface seawater and decreased with the depth. The mixing ratios of COS, DMS, and CS₂ in

* Corresponding author at: Key Laboratory of Marine Chemistry Theory and Technology, Ministry of Education, Ocean University of China, 238 Songling Road, Qingdao 266100, China. E-mail address: gpyang@mail.ouc.edu.cn (G.-P. Yang)

[†]These authors contributed equally to this work and should be considered co-first authors.

21 the atmosphere were 255.9–620.2 pptv, 1.3–191.2 pptv, and 5.2–698.8 pptv during spring and 394.6–850.1 pptv,
22 10.3–464.3 pptv, and 15.3–672.7 pptv in summer, respectively. The ratios of mean oceanic concentrations and
23 atmospheric mixing ratios for summer to spring in COS, DMS, and CS₂ were 1.8, 3.1, 3.7 and 1.6, 4.6, 1.5, respectively.
24 The ratios of the mean sea-to-air fluxes for summer to spring in COS, DMS, and CS₂ were 1.2, 2.1, and 4.3. The sea-
25 to-air fluxes of VSCs indicated that the marginal seas are important sources of VSCs in the atmosphere. The results
26 provide help with a better understanding of the contribution of VSCs in marginal seas.

27 **Keywords:** Volatile organic sulfur compound; Carbonyl sulfide; Dimethyl sulfide; Carbon disulfide

28 **1 Introduction**

29 Carbonyl sulfide (COS), dimethyl sulfide (DMS), and carbon disulfide (CS₂) are three major volatile organic sulfur
30 compounds (VSCs) in seawater and the marine atmosphere. Their biogeochemical cycles are closely related to climate
31 change (Charlson et al., 1987; Li et al., 2022). VSCs contribute to the formation of atmospheric cloud condensation
32 nuclei (CCN) and sulfate aerosols, significantly affecting the global radiation budget and ozone concentration
33 (Andreae and Crutzen, 1997). Hence, interest in the distribution, production, and chemistry of VSCs has grown in
34 recent years (Lennartz et al., 2017; Lennartz et al., 2020; Li et al., 2022; Remaud et al., 2022; Whelan et al., 2018;
35 Yang et al., 2008; Yu et al., 2022). **Production and loss processes of COS, DMS, and CS₂ have been documented by
36 many researchers in the following manners.**

37 COS has an average tropospheric residence time of 2–7 years and is the most abundant and widely distributed
38 reduced sulfur trace gas in the atmosphere (Brühl et al., 2012). COS can be converted to sulfate aerosols in the
39 stratosphere, affecting the Earth's radiation balance (Crutzen, 1976). Atmospheric COS originates directly from
40 oceanic emissions and indirectly from the oxidation of DMS and CS₂ (Kettle et al., 2002; Lennartz et al., 2020).
41 Uptake by terrestrial vegetation and soil is the most important sink of atmospheric COS (Kettle et al., 2002; Maignan
42 et al., 2021). Therefore, COS can be used as a proxy for estimating the photosynthesis rate in ecosystems (Campbell
43 et al., 2008). COS production is dependent on UV radiation, chromophoric dissolved organic matter (CDOM), cysteine,
44 and nitrate concentration (Lennartz et al., 2021; Li et al., 2022). Some studies have indicated that the ocean is a COS
45 source (Chin and Davis, 1993; Yu et al., 2022), whereas others have shown that the ocean is a COS sink (Zhu et al.,
46 2019).

47 Atmospheric DMS can react with OH and NO₃ radicals to form SO₂ and methane sulfonic acid (MSA, CH₃SO₃H),
48 creating non-sea salt sulfates (nss-SO₄²⁻), which contribute to acid deposition and CCN (Charlson et al., 1987). DMS
49 is the predominant biogenic sulfur originating from dimethylsulfoniopropionate (DMSP), predominantly produced by
50 bacteria and phytoplankton (Curson et al., 2017; Keller et al., 1989). DMSP lyase from phytoplankton and bacteria
51 can convert DMSP to DMS (Reisch et al., 2011). The community composition of phytoplankton and bacteria can
52 affect the net DMSP concentrations via synthesis and degradation (O'Brien et al., 2022, Zhao et al., 2021). DMS

53 entering the atmosphere via sea-to-air exchange accounts for about 50% of all natural sulfur releases (Cline and Bates,
54 1983).

55 CS₂ is the key precursor of COS, and 82% COS is the oxidation production of CS₂ (Lennartz et al., 2020).
56 Photochemical reaction with dissolved organic matter (DOM) is a principal source of CS₂ in seawater (Xie et al.,
57 1998). The photochemical reaction of DOM generates excited triplet states of chromophoric dissolved organic matter
58 (³CDOM*), singlet oxygen (¹O₂), hydrogen peroxide (H₂O₂), and hydroxyl radical (·OH). These reactive species
59 subsequently interact with DMS, resulting in the production of CS₂ (Modiri Gharehveran and Shah, 2021). The
60 oxidation reaction involving the OH radicals and CS₂ is a substantial contributor to the generation of SO₂, which
61 subsequently leads to the production of acid rain (Logan et al., 1979). Anthropogenic CS₂ sources include rayon and/or
62 aluminum production, fuel combustion, oil refineries, and coal combustion (Campbell et al., 2015; Zumkehr et al.,
63 2018).

64 Two different approaches (ice core and isotope measurements) were used to evaluate anthropogenic COS emissions
65 (Aydin et al., 2020; Hattori et al., 2020). The latter study and a modeling approach used by Remaud et al. (2022)
66 observed a gradient of anthropogenic COS in East Asia. Anthropogenic COS is initially emitted as CS₂ and oxidized
67 by OH to COS in the atmosphere (Kettle et al., 2002). The production and loss of DMS involve phytoplankton and
68 bacteria synthesis, zooplankton grazing, bacterial degradation, and sea-air diffusion (Schäfer et al., 2010). COS and
69 CS₂ production are related to photo-oxidation and/or photochemical reactions (Lennartz et al., 2020; Xie et al., 1998).
70 However, the production and loss mechanisms remain unclear.

71 The Yellow Sea (YS) and Bohai Sea (BS) are semi-enclosed seas in the northwestern Pacific Ocean. The BS coastal
72 current, YS coastal current, and YS warm current substantially affect the hydrological characteristics of this area
73 (Chen, 2009), potentially altering the VSC distributions via water mass exchanges. In addition, the Yellow Sea Cold
74 Water Mass (YSCWM), a seasonal hydrological phenomenon located in the 35°N transect, forms, peaks, and
75 disappears in spring, summer, and after September, respectively (Zhang et al., 2014). In this study, we investigate the
76 spatial distributions and seasonal variability of COS, DMS, and CS₂ in the seawater and overlying atmosphere of the

77 YS and BS and the effects of the YSCWM (the 35°N transect) on the VSC distributions to better understand the
78 distributions and impact factors of VSCs in Chinese marginal seas.

79 **2 Materials and methods**

80 **2.1 Sampling**

81 Two cruises were conducted aboard the R/V “Dong Fang Hong 2” in the YS and BS from 27 March to 16 April
82 (spring) 2018 and from 24 July to 8 August (summer) 2018. The sampling stations are shown in Fig. 1. Surface and
83 depth seawater samples were collected using 12 L Niskin bottles mounted on a Seabird 911 conductivity-temperature-
84 depth (CTD) rosette. **Surface seawater was sampled at a depth of 3–5 m.** The seawater was slowly siphoned from the
85 Niskin bottles into 100 mL glass jaw bottles (CNW Technologies GmbH, GER) via a translucent silicone tube. The
86 seawater was allowed to overflow the sampling bottle by twice its volume before the silicone tube was gently removed,
87 and the bottle was immediately sealed with an aluminum cap containing a Teflon-lined butyl rubber septum without
88 any headspace. Subsequently, the concentrations of oceanic VSCs were immediately measured on the ship. The
89 environmental and hydrological parameters such as seawater temperature and salinity were measured simultaneously
90 by the CTD equipment.

91 Atmospheric VSC samples were collected using cleaned and vacuumed SilcoCan canisters (Restek, USA) in the
92 windward direction approximately 10 m above the ocean. The stability of VSCs in fused silica-lined canisters has
93 been verified during storage for 16 d at room temperature (Brown et al., 2015). The atmospheric samples were
94 analyzed immediately after being brought back to the laboratory.

95 **2.2 Analytical procedures**

96 The VSC concentrations in the seawater were measured using a gas chromatograph (GC) (Agilent 7890A, USA) with
97 a flame photometric detector (FPD). The atmospheric VSC mixing ratios were measured using a GC equipped with a
98 mass spectrometer (GC-MS) (Agilent 7890A/5975C, USA) using the methods of Inomata et al. (2006) and Staubes
99 and Georgii (1993), respectively. A CP-Sil 5 CB column (30 m × 0.32 mm × 4.0 μm, Agilent Technologies, USA)
100 was used to separate the three VSCs. Standard VSC gases with mixing ratios of 1 ppmv were bought from Beijing
101 Minnick Analytical Instrument Equipment Center. Qualitative analysis was conducted by comparing the results with

102 the retention times of the standards, and quantitative analysis was conducted by diluting the VSC standard gases to 1
103 ppbv and 5 ppbv using a 2202A dynamic dilution meter (Nutech, USA) and injecting different volumes of the diluted
104 VSC standards into the GC using a gas-tight syringe. The VSC mixing ratios were calculated after calibration using
105 standard gases (Fig. S1).

106 The VSC concentrations in seawater were determined using a cryogenic purge-and-trap system coupled with the
107 GC-FPD. A 30 mL seawater sample was injected into a glass bubbling chamber with a gas-tight syringe (SGE,
108 Australia). The VSCs were extracted from the seawater with high purity N₂ at a rate of 60 mL min⁻¹ for 15 min and
109 passed through an anhydrous CaCl₂-filled drying tube and a 100% degreased cotton-filled 1/4 Teflon tube to remove
110 water and oxides. Subsequently, the VSC gases were passed through a six-way valve and trapped in a loop of the 1/16
111 Teflon capture tube immersed in liquid nitrogen. After all VSCs had been purged from the seawater, the capture tube
112 was removed from the liquid nitrogen and placed into hot water (> 90 °C) to desorb the trapped VSCs. The VSCs gases
113 were carried into the GC by N₂ and detected by the FPD. The column temperature was programmed with an initial
114 temperature of 55 °C, followed by an increase to 100 °C at 10 °C min⁻¹ and a final increase to 150 °C at 15 °C min⁻¹.
115 The inlet and detector temperatures were 150 °C and 160 °C, respectively, and the split ratio of pure N₂ was 10:1. The
116 detection limits of the method for COS, DMS, and CS₂ were 33 pg, 387 pg, and 22 pg and the measurement precision
117 was 5.59%–11.70% (Tian et al., 2005). The DMS concentrations in seawater were obtained from Zhang et al. (2023).

118 The mixing ratios of atmospheric VSCs were analyzed using an Entech 7100 pre-concentrator (Nutech, USA)
119 coupled with GC-MS. The sample SilcoCan canister was connected to the pre-concentrator, and 200 mL of gas was
120 drawn into the preconcentration system with a three-stage cold trap (Fig. S1). The pre-concentrator parameters of the
121 three-stage cold trap are listed in Table S1. The first trap removes N₂, O₂, and H₂O (g) from the atmospheric samples,
122 and the second trap eliminates CO₂. The third trap is used to separate the three VSCs and obtain better peak shapes.
123 The temperature programming of the column was the same as for the seawater samples. In addition, the temperature
124 of the quadrupole and ion source were 110 °C and 230 °C, respectively, and the electron ionization source was run at
125 70 eV. The carrier gas had a split ratio of 10:1 and a flow rate of 2.0 mL min⁻¹. Qualitative and quantitative analyses
126 of the VSCs were conducted using the full scan mode (SCAN) and the selected ion monitoring mode (SIM). The
127 mass-to-charge ratios (*m/z*) for COS, DMS, and CS₂ were 60, 62, and 76, respectively. The detection limit of the VSCs

128 was 0.1–0.5 pptv (Zhu et al., 2017).

129 **2.3 Calculation of sea-to-air fluxes of VSCs**

130 The sea-to-air fluxes of the VSCs were calculated using the model established by Liss and Slater (1974): $F = k_w(c_w -$
131 $c_g/H)$, where F is the sea-to-air flux of VSCs ($\mu\text{mol m}^{-2} \text{d}^{-1}$); k_w is the VSC transfer velocity (m d^{-1}); c_w and c_g are the
132 equilibrium concentrations of VSCs in the surface seawater and the atmosphere (nmol L^{-1}), respectively; and H is
133 Henry's constant calculated using the equation listed in Table S2 (De Bruyn et al., 1995; Dacey et al., 1984). It was
134 converted to a dimensionless constant using the equation proposed by Sander (2015). k_w was calculated from the wind
135 speed, and the sea surface temperature was obtained by the N2000 method (Nightingale et al., 2000). **The C_g of DMS**
136 **is assumed to be zero in this study. This is based on the fact that atmospheric mixing ratios of DMS are typically**
137 **several orders of magnitude lower than concentrations in seawater (Turner et al., 1996).** We used the calculation
138 developed by Kettle et al. (2001).

139 **2.4 Measurements of Chl *a*, nutrients, and dissolved organic carbon**

140 The seawater samples for the analysis of the Chl *a* concentrations were filtered through Whatman GF/F filters, and
141 the filtrate was stored in darkness at $-20\text{ }^\circ\text{C}$. Then, Chl *a* was extracted with 90% acetone for 24 h at $4\text{ }^\circ\text{C}$ in darkness.
142 The Chl *a* concentrations were determined following the method of Parsons et al. (1984) with a fluorescence
143 spectrophotometer (F-4500, Hitachi) at excitation/emission wavelengths of 436 nm/670 nm. The seawater was filtered
144 through Whatman GF/F filters ($0.7\text{ }\mu\text{m}$), and the filtered water samples were stored at $-20\text{ }^\circ\text{C}$ before nutrient (nitrate,
145 phosphate, and silicate) analysis. A Technicon Autoanalyser AAII (SEAL Analytical, UK) was used to measure the
146 nitrate, phosphate, and silicate concentrations. The nitrate, phosphate, and silicate data were provided by the open
147 research cruise supported by the National Natural Science Foundation (NSFC) Shiptime Sharing Project.

148 The dissolved organic carbon (DOC) concentrations were measured using the method of Chen et al. (2021). The
149 seawater was filtered through Whatman GF/F filters (pre-combusted at $500\text{ }^\circ\text{C}$ for 4 h), and the filtrate was stored at
150 $-20\text{ }^\circ\text{C}$ for DOC analysis. The DOC concentrations were determined by a total organic carbon analyzer (Shimadzu
151 TOC-VCPH) after adding two drops of 12 mol/L HCl.

152 **2.5 Data analysis**

153 SPSS 24.0 software (SPSS Inc., Chicago, IL, USA) was used to analyze the relationships between the environmental
154 factors and the concentrations and mixing ratios of the three VSCs in seawater and the atmosphere during spring and
155 summer.

156 **3 Results**

157 **3.1 Spatial distributions of COS, DMS, and CS₂ in surface seawater**

158 **3.1.1 Spring distributions**

159 The temperature in the surface seawater showed a decreasing trend from south to north, and the salinity increased
160 from the inshore to the offshore sites due to the influences of the YS warm current, Yalu River, and Yellow River
161 (Fig. 2). The Chl *a* concentrations in the surface water of the BS and YS in the spring were 0.17–4.45 $\mu\text{g L}^{-1}$ with an
162 average of $1.19 \pm 0.96 \mu\text{g L}^{-1}$. The highest Chl *a* concentration occurred at station B39 in the BS (Fig. 2), which may
163 be related to the enhanced phytoplankton growth due to the abundance of nutrients resulting from a seawater exchange
164 between the BS and YS. In addition, high Chl *a* concentrations were observed in the central area of the southern YS.

165 The concentrations of COS, DMS, and CS₂ in the surface seawater of the BS and YS during spring were 0.14–0.42,
166 0.41–7.74, and 0.01–0.18 nmol L^{-1} , with mean values of 0.24 ± 0.06 , 1.74 ± 1.61 , and $0.07 \pm 0.05 \text{ nmol L}^{-1}$,
167 respectively (Fig. 2). The high COS concentrations during the spring occurred in the YS (Fig. 2). The highest COS
168 concentration was observed at station H21, coinciding with a high Chl *a* concentration. The two areas with high
169 concentrations of COS in the central waters of the southern YS overlapped with areas with high Chl *a* concentrations.
170 High DMS concentrations existed in the coastal waters of the southern Shandong Peninsula, as well as at station B21
171 in the central part of the northern YS. The distribution of CS₂ in seawater exhibited a decreasing trend from inshore
172 to offshore (Fig. 2). High CS₂ concentrations appeared at stations H18 and H19 in the coastal waters of YSCWM (Fig.
173 2). There was also a high CS₂ concentration at station B30 near the shore of the Liaodong Peninsula (Fig. 2).

174 **3.1.2 Summer distributions**

175 The temperature and salinity in the BS and YS in summer were relatively high, and high Chl *a* concentrations were
176 concentrated in coastal waters (Fig. 3). The Chl *a* concentrations in the seawater during summer were 0.10–4.74 μg
177 L^{-1} with an average of $1.60 \pm 1.19 \mu\text{g L}^{-1}$. Station B43 near the Yellow River estuary and Laizhou Bay had the highest

178 Chl *a* concentration, which may have been due to the abundance of nutrients (nitrate: 5.85 $\mu\text{mol L}^{-1}$, silicate: 17 μmol
179 L^{-1}) carried by nearby rivers or coastal currents (Figs. 3 and S2). Low salinities and high nitrate and Chl *a*
180 concentrations occurred at Stations H32, H34, and H35 in the northeast of the Yangtze River Estuary and at Stations
181 B66 and B68 near the Laizhou Bay and Yellow River Estuary (Figs. 3 and S2).

182 The concentrations of COS, DMS, and CS₂ in the surface water of the BS and YS during summer were 0.32–0.61,
183 1.31–18.12, and 0.01–0.65 nmol L^{-1} , with mean values of 0.44 ± 0.06 , 5.43 ± 3.60 , and 0.26 ± 0.15 nmol L^{-1} ,
184 respectively (Fig. 3). **The ratios of the mean concentrations between summer and spring for Chl *a*, COS, DMS, and**
185 **CS₂ were 1.3, 1.8, 3.1, and 3.7, respectively.** High COS concentrations were observed at stations B38 and B54 in the
186 BS during summer. In addition, COS had a high concentration at station H25 in the central part of the southern YS,
187 close to a location with a high CS₂ concentration (Fig. 3). High DMS concentrations were common in the northern BS
188 and were generally coincident with high Chl *a* levels. However, high Chl *a* and DMS concentrations were found in
189 the coastal waters of the Yangtze River Estuary due to the Changjiang diluted water. In addition, the DMS
190 concentration was high at station H12 (Fig. 3). There were high CS₂ concentrations in the northeastern area of the
191 Yangtze River estuary (Fig. 3).

192 **3.2 Depth distributions of COS, DMS, and CS₂ in seawater**

193 **3.2.1 Depth distributions in spring**

194 The temperature and Chl *a* decreased from the surface to the bottom seawater (Fig. 4). **The ratios of the mean**
195 **concentrations between the surface and greater depths (> 60 m) were 5.4, 5.1, 5.9, and 8.9 for Chl *a*, COS, DMS, and**
196 **CS₂, respectively** (Fig. 4). Consistent with the Chl *a* distribution, the depth distribution of DMS in the seawater
197 decreased from the euphotic zone to the bottom seawater (Fig. 4). High COS concentrations occurred in the surface
198 seawater and decreased with the depth, and the lowest concentrations occurred in the bottom waters. CS₂ exhibited
199 depth gradients at most stations during spring, with higher concentrations at the surface, except for station H15 where
200 the CS₂ concentrations were high in the bottom seawater.

201 **3.2.2 Depth distributions in summer**

202 The YSCWM affected the depth distributions in summer in the 35°N transect. Substantial temperature differences

203 occurred between the surface and bottom seawater in summer, and stratification in the water bodies was observed (Fig.
204 5). A distinct thermocline existed at a depth of 20 m, indicating the formation of the YSCWM (Fig. 5). All high Chl
205 *a* concentrations in the surveyed area of the BS and YS during summer occurred in the euphotic zone, and the highest
206 concentrations occurred in waters at depths of 10–20 m (Fig. 5). **The ratio of the mean Chl *a* concentration at depths
207 of 10–20 m to depths > 60 m was 5.4.** The depth distribution of DMS in seawater during summer decreased from the
208 surface to the bottom seawater (Fig. 5). A significant depth gradient in the COS and CS₂ concentrations occurred at
209 most stations, exhibiting decreases with the increasing depth. **The ratios of the mean concentrations of COS, DMS,
210 and CS₂ between the surface and depths > 60 m were 12.0, 8.6, and 11.5, respectively.** However, the COS
211 concentration was high in the bottom waters of station H16 (0.465 nmol L⁻¹) (Fig. 5). **The ratios of the mean
212 concentrations of Chl *a*, COS, DMS, and CS₂ of all samples at different depths between summer and spring were 2.2,
213 1.0, 5.6, and 2.0, respectively.**

214 **3.3 VSCs in the atmosphere**

215 **3.3.1 Spring**

216 The mixing ratios of COS, DMS, and CS₂ in the atmosphere overlying the BS and YS in spring were in the ranges of
217 255.9–620.2 pptv, 1.3–191.2 pptv, and 5.2–698.8 pptv (Figs. 6a-6c), and their mean mixing ratios were 345.6 ± 79.2
218 pptv, 47.5 ± 49.8 pptv, and 113.2 ± 172.3 pptv, respectively. The decreasing order of the mean mixing ratios of the
219 three VSCs in the atmosphere during spring was COS > CS₂ > DMS. The highest mixing ratio of atmospheric COS
220 occurred at station B72 (Fig. 6a) near the northern Shandong Peninsula. The highest atmospheric DMS mixing ratio
221 was observed at station B08 (Fig. 6b). The DMS concentration in the seawater (Fig. 2) was not as high as that in the
222 atmosphere at station B49 (Fig. 6b). According to the 72 h backward trajectory map (Fig. S3), the air mass over station
223 B49 had migrated from the land to the ocean, passing through Beijing, Tianjin, and other densely populated areas.
224 **The air mass over station B47 differed slightly from that over station B49 as it traversed the land of Liaoning province
225 (12 h and 24 h backward trajectories in Fig. S3).** The lowest atmospheric DMS mixing ratio was observed at station
226 B47 (Fig. 6b), probably due to the low DMS concentration in seawater (0.5 nmol L⁻¹) and the loss across the land. The
227 highest atmospheric DMS mixing ratio occurred at station B08 (Fig. 6b). In addition, there were high mixing ratios of

228 CS₂ at stations in the BS, such as B57, B60, and B72, and low mixing ratios at stations B17 and B21 in the northern
229 YS (Fig. 6c).

230 3.3.2 Summer

231 The mixing ratios of COS, DMS, and CS₂ in summer ranged from 394.6 to 850.1 pptv, from 10.3 to 464.3 pptv, and
232 from 15.3 to 672.7 pptv, with mean values of 563.8 ± 168.9 pptv, 216.6 ± 136.0 pptv, and 164.4 ± 225.5 pptv,
233 respectively (Fig. 6d–6f). The order of the three VSCs in terms of the mean mixing ratios in the atmosphere during
234 summer was COS > DMS > CS₂. **The ratios of the mean mixing ratios for atmospheric COS, DMS, and CS₂ between**
235 **summer and spring were 1.6, 4.6, and 1.5, respectively.** The three VSCs in the atmosphere over the BS and YS had
236 similar spatial distributions. COS and DMS exhibited the highest mixing ratios at station B64 (Fig. 6d and 6e). The
237 highest mixing ratio of CS₂ in summer appeared at station B49 near the shore, and the lowest one occurred far from
238 shore at station H09 (Fig. 6f). The air masses over stations B49, B64, and H09 had migrated from the land, land, and
239 ocean, respectively (Fig. S3). The distributions of CS₂ showed a decreasing trend from inshore to offshore (Fig. 6f).

240 3.4 Relationships between environmental factors and COS, DMS, and CS₂ concentrations

241 A significant correlation was found between the DMS and CS₂ concentrations in the surface seawater in spring ($P <$
242 0.05) and summer ($P < 0.01$) (Table 1). A positive correlation occurred between the COS and DOC concentrations in
243 seawater ($P < 0.05$) and between the CS₂ and Chl *a* concentrations in seawater ($P < 0.05$) during summer (Table 1).
244 There was a significant correlation between the atmospheric COS and CS₂ mixing ratios in spring and summer ($P <$
245 0.01 , Table 1).

246 3.5 Sea-to-air fluxes of VSCs

247 3.5.1 Spring

248 The sea-to-air fluxes of COS, DMS, and CS₂ in spring were 0.03–1.59, 0.06–25.40, and 0.003–0.30 $\mu\text{mol m}^{-2} \text{d}^{-1}$, with
249 averages of 0.50 ± 0.38 , 2.99 ± 4.24 , and 0.09 ± 0.08 $\mu\text{mol m}^{-2} \text{d}^{-1}$, respectively (Fig. 7). The highest COS sea-to-air
250 flux was observed at station B36, which had a high wind speed (11.3 m s^{-1}). In comparison, the lowest COS sea-to-air
251 flux occurred at station B12, where the minimum wind speed occurred (1.5 m s^{-1}). The lowest sea-to-air fluxes of
252 DMS and CS₂ occurred at stations H01 and B41 (Fig. 7), where the wind speeds were 0.4 m s^{-1} and 2 m s^{-1} , respectively.

253 The highest DMS and CS₂ sea-to-air fluxes appeared at stations HS4 and B68, respectively, due to high wind speeds
254 and high DMS and CS₂ concentrations in seawater (Fig. 7).

255 **3.5.2 Summer**

256 The sea-to-air fluxes of COS, DMS, and CS₂ in summer were 0.06–1.51, 0.10–25.44, and 0.02–0.99 $\mu\text{mol m}^{-2} \text{d}^{-1}$,
257 with averages of 0.60 ± 0.59 , 6.26 ± 6.27 , and $0.39 \pm 0.42 \mu\text{mol m}^{-2} \text{d}^{-1}$, respectively, (Fig. 8). **The ratios of the mean**
258 **sea-to-air fluxes for COS, DMS, and CS₂ between summer and spring were 1.2, 2.1, and 4.3, respectively.** Consistent
259 with their order in seawater, the order of the sea-to-air fluxes of the VSCs was DMS > COS > CS₂. The lowest sea-
260 to-air fluxes of COS, DMS, and CS₂ in summer occurred at stations B64, B05, and B57, which had the low wind
261 speeds of 1 m s^{-1} , 0.4 m s^{-1} , and 1.1 m s^{-1} , respectively and low seawater VSC concentrations. The highest sea-to-air
262 flux of COS and DMS occurred at stations B70 and H14, respectively, coinciding with high wind speeds and high
263 COS and DMS concentrations in seawater (Fig. 8). The maximum CS₂ sea-to-air flux appeared at station H09, where
264 the concentration of CS₂ in seawater was 0.31 nmol L^{-1} (Fig. 8).

265 **4 Discussion**

266 **4.1 Spatial and depth distributions and seasonal variations in VSCs in seawater**

267 **4.1.1 Spatial distributions of VSCs and the impact factors**

268 The COS concentrations in this study were similar to those in six tidal European estuaries (Scheldt, Gironde, Rhine,
269 Elbe, Ems, and Loire) (0.22 nmol L^{-1}) (Sciare et al., 2002), the DMS concentrations were lower than previous
270 observations in the BS and YS in autumn (3.92 nmol L^{-1}) (Yang et al., 2014), and the CS₂ concentrations were lower
271 than those in the coastal waters off the eastern coast of the United States ($0.004\text{--}0.51 \text{ nmol L}^{-1}$) (Kim and Andreae,
272 1992). Besides, the VSC concentrations in the seawater of the BS and YS were significantly higher than those in
273 oceanic areas, such as the North Atlantic Ocean (Simó et al., 1997; Ulshöfer et al., 1995). The higher CDOM
274 concentrations in the nearshore waters may be the reason for the difference (Gueguen et al., 2005). Zepp and Andreae
275 (1994) demonstrated that photosensitized reaction of organosulfur compounds contributed to the production of COS.
276 The reaction rates in coastal waters may be higher than those in open sea. Our results showed that the average COS,
277 DMS, and CS₂ concentrations in the surface seawater of the BS and YS during summer were higher than those in the
278 Changjiang estuary and the adjacent East China Sea (Yu et al., 2022). The reasons may be different sea areas,

279 temperatures, and industrial production. The mean concentrations of COS, DMS, and CS₂ in the surface seawater of
280 the BS and YS during both spring and summer were 0.34, 3.41, 0.16 nmol L⁻¹, respectively. The mean COS and CS₂
281 concentrations were approximately one order of magnitude higher than the global values reported by Lennartz et al.
282 (2020), which were 32.3 pmol L⁻¹ and 15.7 pmol L⁻¹. Lennartz et al. (2020) highlighted that the COS concentrations
283 in estuaries and shelves were 10–1000 fold higher than those in oligotrophic waters. This disparity in concentrations
284 may account for the discrepancies observed between our findings and global values. In comparison, the mean DMS
285 concentration was similar with the value reported by Hulswar et al. (2022), which was 2.26 nmol L⁻¹.

286 Different production and consumption mechanisms resulted in different spatial distributions of COS, DMS, and
287 CS₂. DMS and DMSP concentrations are related to the composition and abundance of phytoplankton (Kurian et al.,
288 2020; Naik et al., 2020; O'Brien et al., 2022; Yu et al., 2023). The highest DMS concentrations at station B21 in spring
289 coincided with high Chl *a* concentrations (Fig. 2). Low salinities (< 30) occurred at stations H25, H26, H34, H35,
290 B43, B66, and B68 due to river water discharge from the Yangtze River Estuary, Yellow River, and Laizhou Bay in
291 summer, consistent with the high nitrate, silicate, Chl *a*, and DMS concentrations (Figs. 3 and S2). High CS₂
292 concentrations in the coastal waters of the Yellow River estuary and at stations H18, H19, and B30 in spring may be
293 due to high CDOM carried by the YS coastal current and Yellow River and terrestrial input. The significant correlation
294 between the DMS and CS₂ concentrations in the surface seawater was consistent with the results of Ferek and Andreae
295 (1983) and Yu et al. (2022). DMS in seawater is primarily derived from the degradation of DMSP, which is released
296 from algal cell lysis (O'Brien et al., 2022). Moreover, the algae decay increased the CS₂ emission rate due to the
297 degradation of sulfur-containing amino acids (Wang et al., 2023). The commonality of their sources resulted in a high
298 correlation between the DMS and CS₂ concentrations in seawater. Xie et al. (1998) pointed out that CS₂ has a
299 photochemical production mechanism similar to that of COS. Both are primarily produced by photochemical reactions
300 of thiol-containing compounds, such as methyl mercaptan (MeSH) or glutathione, under the catalysis of CDOM.
301 Terrestrial CDOM has higher photochemical reactivity and is more conducive to the photochemical generation of CS₂
302 (Xie et al., 1998). COS production rates increase with an increase in the absorption coefficient at 350 nm (*a*₃₅₀) (Li et
303 al., 2022). Uher and Andreae (1997) showed that the COS concentration in seawater was significantly correlated with
304 the CDOM concentration. The positive correlation between the COS and DOC concentrations in seawater during
305 summer in this study suggested that COS was produced by the photochemical reaction of CDOM. COS and CS₂ are
306 formed via a reaction between cysteine and intermediates (i.e., CDOM, [•]OH) (Chu et al., 2016; Du et al., 2017; Modiri

307 Gharehveran et al., 2020). Modiri Gharehveran and Shah (2021) showed that DOM could photochemically produce
308 $^3\text{CDOM}^*$, $^1\text{O}_2$, H_2O_2 , and $^{\bullet}\text{OH}$ by sunlight reacting with DMS, forming a sulfur- or carbon-centered radical and
309 subsequently COS and CS_2 . Li et al. (2022) demonstrated that a high nitrate concentration resulted in a high COS
310 production rate. The high COS concentrations at stations H25 and B43 during summer coincided with high nitrate
311 concentrations (Figs. 3 and S2). However, no significant correlations were found between the COS and nitrate
312 concentrations during summer (Tables 1).

313 **4.1.2 Depth distributions of VSCs and impact factors**

314 The depth distributions of DMS, COS and CS_2 showed similar patterns; their concentrations decreased with increasing
315 depth, in agreement with the results of Yu et al. (2022). Yu et al. (2023) also showed that the DMS concentrations in
316 the 35°N transect of the BS and YS in autumn decreased with an increase in seawater depth. The highest Chl *a*
317 concentrations during summer occurred at depths of 10–20 m. This result was attributed to the abundance of nutrients
318 and suitable water temperatures near the thermocline, benefitting phytoplankton growth. Yu et al. (2021) reported that
319 the highest DMSP-consuming bacterial abundance and DMSP lyase activity at the 35°N transect in the summer of
320 2013 occurred at depths of 10–15 m, consistent with our Chl *a* concentrations. DMS originates primarily from
321 phytoplankton; thus, its concentration trend is similar to that of Chl *a*. COS and CS_2 in seawater are predominantly
322 derived from photochemical reactions of organic sulfides catalyzed by CDOM; therefore, light is the limiting factor
323 for their production in seawater (Uher and Andreae, 1997). Ulshöfer et al. (1996) studied the depth distribution of
324 COS in seawater and found that high COS concentrations occurred in the euphotic zone. The high COS concentrations
325 in the surface seawater in this study may be attributed to the photochemical production reactions of CS_2 and COS in
326 the euphotic zone because they are dependent on light (Flöck et al., 1997; Xie et al., 1998). The addition of
327 photosensitizers-natural DOM and commercial humic acid (HA) photo-catalyzed glutathione (GSH) and cysteine, and
328 enhanced the COS formation (Flöck et al., 1997). An excited triplet state CDOM ($^3\text{CDOM}^*$) is produced by COS in
329 the presence of ultraviolet light (Li et al., 2022). **In addition, the loss processes include exhalation, downward mixing,**
330 **and hydrolysis, with hydrolysis being identified as the predominant sink (Xu et al., 2001). We speculate that slow**
331 **hydrolysis rate may be another reason accounting for the high COS concentrations in the surface seawater.** Hobe et
332 al. (2001) stated that the non-photochemical production of COS is critical for the global budget. Consistent with Hobe
333 et al. (2001), the high COS concentration in the bottom waters at station H16 in summer may be related to the non-
334 photochemical production of COS or release by underlying sediments. Consistent with our CS_2 results, Xie et al. (1998)

335 showed that the CS₂ concentrations decreased with the depth, coinciding with solar radiation changes. Decreased
336 photochemical reaction due to decreasing solar radiation with water depth may explain the vertical distribution of CS₂
337 (Xie et al., 1998). Similar to the results of Xie et al. (1998), the high CS₂ concentrations in the bottom seawater at
338 station H15 in spring may be attributable to a sedimentary source.

339 **4.1.3 Seasonal and diurnal variations in VSCs in seawater**

340 The VSCs in seawater exhibited significant seasonal differences (VSCs in summer > VSCs in spring) in this study.
341 Similar seasonal variations in COS were also observed by Xu et al. (2001), who found that the COS concentrations in
342 South Africa were higher in summer than in autumn. In addition, observations by Weiss et al. (1995) showed that the
343 COS concentrations in the seawater of the Atlantic and Pacific Oceans were very low in winter. Xu et al. (2001)
344 concluded that warmer seasons and high biological productivity resulted in enhanced COS concentrations. The
345 significant correlation between the oceanic COS concentrations and the temperatures in spring (Table 1) can prove
346 this. Xie et al. (1998) showed that the order of the CS₂ production rates was summer > spring > fall > winter. The
347 significant positive correlations between the CS₂ and Chl *a* concentrations during summer may explain the higher CS₂
348 concentration in seawater during summer than during spring in this study. Similar to the seasonal changes in Chl *a*,
349 the DMS concentrations were higher in summer than in spring. A higher phytoplankton biomass in summer has been
350 linked to higher DMS concentrations in summer than in autumn (Yang et al., 2015). In addition, diurnal variations in
351 the COS concentrations in seawater (high during the daytime and low at night) were reported (Ferek and Andreae,
352 1984; Lennartz et al., 2017; Xu et al., 2001). COS photoproduction via photochemical reactions is more rapid than
353 hydrolysis during the daytime (Xu et al., 2001). **Furthermore**, the COS concentration depends on the light intensity
354 (Ferek and Andreae, 1984). **Therefore, the sampling time can influence the measured COS concentrations in the**
355 **seawater.**

356 **4.2 VSCs in the atmosphere**

357 **The mean mixing ratios of COS and CS₂ in the atmosphere overlying the BS and YS during both spring and summer**
358 **were 411.0 and 128.6 pptv, respectively. These values were 0.75-fold and 3.05-fold of the global scale values reported**
359 **by Lennartz et al. (2020), which were 548.9 ppt and 42.2 ppt.** Similar to our results for the VSC mixing ratios in the
360 atmosphere during summer, Kettle et al. (2001) found that the COS mixing ratio in the Atlantic Ocean atmosphere
361 was 552 pptv, while Cooper and Saltzman (1993) measured a DMS mixing ratio of 118 pptv. In addition, the mixing

362 ratios of atmospheric CS₂ in this study were similar to those in a polluted atmosphere (Sandalls and Penkett, 1977)
363 but much higher than those in unpolluted atmospheres, such as over the North Atlantic (Cooper and Saltzman, 1993).
364 This finding indicated that industrial production and human activities significantly affect the mixing ratios of CS₂ in
365 the atmosphere. The mean VSC mixing ratios in the atmosphere during summer in this study were all higher than
366 those in the Changjiang estuary and the adjacent East China Sea (Yu et al., 2022), and the Western Pacific during
367 autumn (Xu et al., 2023).

368 No significant correlation was found between the oceanic VSC concentrations and atmospheric VSC mixing ratios
369 (Table 1). The reason may be that VSCs in the atmosphere were not only derived from sea-to-air diffusion but also
370 from anthropogenic sources, such as the soil, incomplete burning of biomass, and industrial releases (Blake et al.,
371 2004; Chin and Davis, 1993; Whelan et al., 2018). Anthropogenic VSC emissions can be evaluated using isotope
372 measurements (Hattori et al., 2020). However, anthropogenic VSCs emissions were not evaluated in this study, and
373 isotope measurements will be obtained in future studies. The highest mixing ratios of atmospheric COS at station B72
374 and DMS at station B08 in spring coincided with anthropogenic emissions and high DMS concentration in seawater,
375 respectively (Fig. 6). The CS₂ generated by industrial activities may have influenced the atmosphere at station B49,
376 which is near industrial cities, such as Tianjin. Chemical production and pharmaceutical industries are large emitters
377 of CS₂ into the atmosphere (Chin and Davis, 1993). CS₂ is the main precursor of COS in the atmosphere, and
378 atmospheric CS₂ is oxidized to COS by radicals such as OH with a conversion efficiency of 0.81 (Chin and Davis,
379 1995). The significant correlation between atmospheric COS and CS₂ in our study (Table 1) demonstrated this.

380 The tropospheric lifetime of COS, CS₂, and DMS were found to be 2–7 years, several days, and approximately 24
381 h, respectively (Lennartz et al., 2020; Khan et al., 2016). Backward trajectories in 12, 24, and 72 h were used to
382 identify the sources of these compounds in our study (Fig. S3). The 72 h backward trajectories showed that air masses
383 from different sources (land or ocean) and passing through different regions may have affected the atmospheric COS,
384 DMS, and CS₂ mixing ratios. Jiang et al. (2021) stated that different sources of air masses might have affected
385 atmospheric DMS oxidation to MSA. The 72 h backward trajectory over station B49 indicated that the high
386 atmospheric DMS mixing ratio was attributable to human activities. The wind direction is from continental Asia to
387 the Pacific in spring. The backward trajectories of B49, B47, and B08 showed that anthropogenic and oceanic DMS
388 emissions accounted for the atmospheric DMS sources. The wind direction of the air mass from the back trajectories

389 of Miyakojima, Yokohama, and Otaru in Japan in winter (January to March) observed by Hattori et al. (2020) was
390 similar to ours in spring (March to April). Hattori et al. (2020) reported that the anthropogenic COS originated
391 primarily from the Chinese industry and was transported by air to southern Japan. The backward trajectory of H09
392 showed that the wind direction was from the south of Taiwan Island in summer, and oceanic sources accounted for
393 the atmospheric DMS. The air masses showed that the highest mixing ratios of COS and DMS at station B64 in
394 summer were caused by terrestrial sources from northeast China and oceanic sources in the BS, respectively. The
395 highest CS₂ mixing ratio in summer at station B49 may be due to the air mass transported from the northeast, i.e.,
396 industrial cities in China.

397 **4.3 Sea-to-air fluxes of VSCs**

398 **The mean sea-to-air fluxes of DMS in spring ($2.99 \mu\text{mol S m}^{-2} \text{d}^{-1}$) and summer ($6.26 \mu\text{mol S m}^{-2} \text{d}^{-1}$) observed in our**
399 **study fell within the range of global DMS fluxes, which ranged from 0 to $10 \mu\text{mol S m}^{-2} \text{d}^{-1}$ (Hulswar et al., 2022).**
400 **The calculated DMS sea-to-air fluxes in our study should be seen as upper limits due to setting the atmospheric mixing**
401 **ratio to be zero.** The spatial variability in the sea-to-air fluxes was consistent with changes in the wind speed because
402 sea-to-air fluxes depend on the transmission velocities of VSCs in seawater, which are related to the wind speed and
403 viscosity of seawater. In addition, the sea-to-air fluxes of all three VSCs were positive in spring and summer, indicating
404 that the seawater was a source of COS, DMS, and CS₂ to the atmosphere through sea-to-air diffusion. Although our
405 findings agree with those of Chin and Davis (1993) and Yu et al. (2022), who showed that the ocean was a major
406 atmospheric source of COS, they conflict with the results of Weiss et al. (1995) and Zhu et al. (2019), who found
407 significant COS undersaturation in some sea areas. Therefore, the ocean may be a sink of atmospheric COS in some
408 areas or at certain times of the year.

409 **5 Conclusions**

410 The COS, DMS, and CS₂ distributions in the surface seawater and marine atmosphere of the BS and YS during spring
411 and summer exhibited significant spatial and seasonal variability. First, the COS, DMS, and CS₂ concentrations were
412 higher in summer than in spring. Second, the COS, DMS, and CS₂ concentrations were the highest in the surface
413 seawater and decreased with the depth. The positive correlation between the oceanic COS and DOC concentrations in
414 summer suggested the photochemical production of COS from CDOM. In addition, the atmospheric VSC mixing
415 ratios of the BS and YS exhibited substantial seasonal differences, with higher mixing ratios in summer than in spring.

416 There was a significant correlation between the atmospheric COS and CS₂ mixing ratios, which may verify the COS
417 production from oxidation of CS₂. The backward trajectories showed that the atmospheric mixing ratios of VSCs were
418 affected by anthropogenic and/or oceanic emissions. Finally, the high sea-to-air fluxes of COS, DMS, and CS₂ in the
419 BS and YS indicated that marginal seas are **important** sources of atmospheric VSCs and may contribute considerably
420 to the global sulfur budget.

421 *Data availability.* Data to support this article are available at <https://doi.org/10.6084/m9.figshare.14971644>.

422 *Author contributions.* All authors were involved in the writing of the paper and approved the final submitted paper.

423 YJ and YL were major contributors to the study's conception, data analysis and drafting of the paper. HZ, LJG and
424 LQ contributed significantly to writing-original draft. YGP contributed to writing-reviewing, and editing.

425 *Competing interests.* The authors declare that they have no conflict of interest.

426 *Acknowledgements.* We are grateful to the captain and crew of the R/V “Dong Fang Hong 2” for their help and
427 cooperation during the in situ investigation.

428 *Financial support.* This work was funded by the National Natural Science Foundation of China (41976038, 41876122),
429 and the National Key Research and Development Program (2016YFA0601301).

430 **References**

431 Andreae, M. O., and Crutzen, P. J.: Atmospheric aerosols: biogeochemical sources and role in atmospheric chemistry,
432 *Science*, 276 (5315), 1052–1058, <https://doi.org/10.1126/science.276.5315.1052>, 1997.

433 Aydin, M., Britten, G. L., Montzka, S. A., Buizert, C., Primeau, F. W., Petrenko, V. V., Battle, M. O., Nicewonger,
434 M. R., Patterson, J., Hmiel, B., and Saltzman, E. S.: Anthropogenic impacts on atmospheric carbonyl sulfide since
435 the 19th century inferred from polar firn air and ice core measurements, *J. Geophys. Res.-Atmos.*, 125(16),
436 e2020JD033074, <https://doi.org/10.1002/essoar.10503126.1>, 2020.

437 Blake, N. J., Streets, D. G., Woo, J.-H., Simpson, I. J., Green, J., Meinardi, S., Kita, K., Atlas, E., Fuelberg, H. E.,
438 Sachse, G., Avery, M. A., Vay, S. A., Talbot, R. W., Dibb, J. E., Bandy, A. R., Thornton, D. C., Rowland, F. S.,
439 and Blake, D. R.: Carbonyl sulfide and carbon disulfide: large-scale distributions over the western Pacific and
440 emissions from Asia during TRACE-P, *J. Geophys. Res.-Atmos.*, 109, D15S05,
441 <https://doi.org/10.1029/2003JD004259>, 2004.

442 Brown, A. S., van der Veen, A. M. H., Arrhenius, K., Murugan, A., Culleton, L. P., Ziel, P. R., and Li, J.: Sampling

443 of gaseous sulfur-containing compounds at low concentrations with a review of best-practice methods for biogas
444 and natural gas applications, *Trac-Trends Anal. Chem.*, 64, 42–52, <https://doi.org/10.1016/j.trac.2014.08.012>, 2015.

445 Brühl, C., Lelieveld, J., Crutzen, P. J., and Tost, H.: The role of carbonyl sulphide as a source of stratospheric sulphate
446 aerosol and its impact on climate, *Atmos. Chem. Phys.*, 12(3), 1239–1253, [http://dx.doi.org/10.5194/acp-12-1239-](http://dx.doi.org/10.5194/acp-12-1239-2012)
447 2012, 2012.

448 Campbell, J. E., Carmichael, G. R., Chai T., Mena-Carrasco, M., Tang, Y., Blake, D. R., Blake, N. J., Vay, S. A.,
449 Collatz, G. J., Baker, I., Berry, J. A., Montzka, S. A., Sweeney, C., Schnoor, J. L., and Stanier, C. O.: Photosynthetic
450 control of atmospheric carbonyl sulfide during the growing season, *Science*, 322, 1085–1088,
451 <https://doi.org/10.1126/science.1164015>, 2008.

452 Campbell, J. E., Whelan, M. E., Seibt U., Smith S. J., Berry, J. A., and Hilton, T. W.: Atmospheric carbonyl sulfide
453 sources from anthropogenic activity: Implications for carbon cycle constraints, *Geophys. Res. Lett.*, 42, 3004–3010,
454 <https://doi.org/10.1002/2015GL063445>, 2015.

455 Charlson, R. J., Lovelock, J. E., Andreae, M. O., and Warren, S. G.: Oceanic phytoplankton, atmospheric sulphur,
456 cloud albedo and climate, *Nature*, 326, 655–661, <https://doi.org/10.1038/326655a0>, 1987.

457 Chen C.-T. A.: Chemical and physical fronts in the Bohai, Yellow and East China seas, *J. Mar. Syst.*, 78(3), 394–410,
458 <https://doi.org/10.1016/j.jmarsys.2008.11.016>, 2009.

459 Chen, Y., Wang, P., Shi, D., Ji, C.-X., Chen, R., Gao, X.-C., and Yang, G.-P.: Distribution and bioavailability of
460 dissolved and particulate organic matter in different water masses of the Southern Yellow Sea and East China Sea,
461 *J. Marine Syst.*, 222, 103596, <https://doi.org/10.1016/j.jmarsys.2021.103596>, 2021.

462 Chin, M., and Davis, D. D.: Global sources and sinks of OCS and CS₂ and their distributions, *Global Biogeochem.*
463 *Cy.*, 7(2), 321–337, <https://doi.org/10.1029/93GB00568>, 1993.

464 Chin, M., and Davis, D. D.: A reanalysis of carbonyl sulfide as a source of stratospheric background sulfur aerosol, *J.*
465 *Geophys. Res.-Atmos.*, 100(D5), 8993–9005, <https://doi.org/10.1029/95JD00275>, 1995.

466 Chu, C., Erickson, P. R., Lundeen, R. A., Stamatelatos, D., Alaimo, P. J., Latch D. E., and McNeill, K.: Photochemical
467 and nonphotochemical transformations of cysteine with dissolved organic matter, *Environ. Sci. Technol.*, 50, 6363–
468 6373, <https://doi.org/10.1021/acs.est.6b01291>, 2016.

469 Cline, J. D., and Bates, T. S.: Dimethyl sulfide in the Equatorial Pacific Ocean: a natural source of sulfur to the
470 atmosphere, *Geophys. Res. Lett.*, 10(10), 949–952, <https://doi.org/10.1029/GL010i010p00949>, 1983.

471 Cooper, D. J., and Saltzman, E. S.: Measurements of atmospheric dimethylsulfide, hydrogen sulfide, and carbon
472 disulfide during GTE/CITE 3, *J. Geophys. Res.-Atmos.*, 98(D12), 23397–23409,
473 <https://doi.org/10.1029/92JD00218>, 1993.

474 Crutzen, P. J.: The possible importance of CSO for the sulfate layer of the stratosphere, *Geophys. Res. Lett.*, 3(2), 73–
475 76, <https://doi.org/10.1029/GL003i002p00073>, 1976.

476 Curson, A. R. J., Liu, J., Bermejo Martínez, A., Green, R. T., Chan, Y., Carrión, O., Williams, B. T., Zhang, S.-H.,
477 Yang, G.-P., Bulman Page, P. C., Zhang, X.-H., and Todd, J. D.: Dimethylsulfoniopropionate biosynthesis in marine
478 bacteria and identification of the key gene in this process, *Nat. Microbiol.*, 2: 17009,
479 <https://doi.org/10.1038/nmicrobiol.2017.9>, 2017.

480 Dacey, J. W. H., Wakeham, S. G., and Howes, B. L.: Henry's law constants for dimethylsulfide in freshwater and
481 seawater, *Geophys. Res. Lett.*, 11, 991–994, <https://doi.org/10.1029/GL011i010p00991>, 1984.

482 De Bruyn, W. J., Swartz, E., Hu, J. H., Shorter, J. A., Davidovits, P., Worsnop, D. R., Zahniser, M. S., and Kolb, C.
483 E.: Henry's law solubilities and Setchenow coefficients for biogenic reduced sulfur species obtained from gas-liquid
484 uptake measurements, *J. Geophys. Res.-Atmos.*, 100, 7245–7251, <https://doi.org/10.1029/95JD00217>, 1995.

485 Du, Q., Mu, Y., Zhang, C., Liu, J., Zhang, Y., and Liu, C.: Photochemical production of carbonyl sulfide, carbon
486 disulfide and dimethyl sulfide in a lake water, *J. Environ. Sci.*, 51, 146–156,
487 <https://doi.org/10.1016/j.jes.2016.08.006>, 2017.

488 Ferek, R. J., and Andreae, M. O.: Photochemical production of carbonyl sulphide in marine surface waters. *Nature*,
489 307, 148–150, <https://doi.org/10.1038/307148a0>, 1984.

490 Ferek, R. J., and Andreae, M. O.: The supersaturation of carbonyl sulfide in surface waters of the Pacific Ocean off
491 Peru, *Geophys. Res. Lett.*, 10(5), 393–396, <https://doi.org/10.1029/GL010I005P00393>, 1983.

492 Flöck, O. R., Andreae, M. O., and Dräger, M.: Environmentally relevant precursors of carbonyl sulfide in aquatic
493 systems, *Mar. Chem.*, 59(1-2), 71–85, [https://doi.org/10.1016/S0304-4203\(97\)00012-1](https://doi.org/10.1016/S0304-4203(97)00012-1), 1997.

494 Guéguen, C., Guo, L., and Tanaka, N.: Distributions and characteristics of colored dissolved organic matter in the

495 Western Arctic Ocean, *Cont. Shelf Res.*, 25, 1195–1207, <https://doi.org/10.1016/j.csr.2005.01.005>, 2005.

496 Hattori, S., Kamezaki, K., and Yoshida, N.: Constraining the atmospheric OCS budget from sulfur isotopes, *Proc.*
497 *Natl. Acad. Sci. U.S.A.*, 117(34), 20447–20452, <https://doi.org/10.1073/pnas.2007260117>, 2020.

498 Hobe, M. V., Cutter, G. A., Kettle, A. J., and Andreae, M. O.: Dark production: a significant source of oceanic COS,
499 *J. Geophys. Res.-Oceans.*, 106(C12), 31217–31226, <https://doi.org/10.1029/2000JC000567>, 2001.

500 Hulswar, S., Sim ó R., Gal í M., Bell, T. G., Lana, A., Inamdar, S., Halloran, P. R., Manville, G., and Mahajan, A. S.:
501 Third revision of the global surface seawater dimethyl sulfide climatology (DMS-Rev3), *Earth Syst. Sci. Data*, 14,
502 2963–2987, <https://doi.org/10.5194/essd-14-2963-2022>, 2022.

503 Inomata, Y., Hayashi, M., Osada, K., and Iwasaka, Y.: Spatial distributions of volatile sulfur compounds in surface
504 seawater and overlying atmosphere in the northwestern Pacific Ocean, eastern Indian Ocean, and Southern Ocean,
505 *Global Biogeochem. Cy.*, 20(2), GB2022, <https://doi.org/10.1029/2005GB002518>, 2006.

506 Jiang, B., Xie, Z., Qiu, Y., Wang, L., Yue, F., Kang, H., Yu, X., and Wu, X.: Modification of the conversion of
507 dimethylsulfide to methanesulfonic acid by anthropogenic pollution as revealed by long-term observations, *ACS*
508 *Earth Space Chem.*, 5, 2839–2845, <https://doi.org/10.1021/acsearthspacechem.1c00222>, 2021.

509 Keller, M. D., Bellows, W. K., and Guillard, R. R. L.: Dimethyl sulfide production in marine phytoplankton, in:
510 *Biogenic sulfur in the environment*, edited by: Millero, F. J., Hershey, J. P., Saltzman, E. S., and Cooper, W. J.,
511 American Chemical Society, Washington, DC, 167–182, <http://dx.doi.org/10.1021/bk-1989-0393.ch011>, 1989.

512 Kettle, A. J., Kuhn, U., von Hobe, M., Kesselmeier, J., and Andreae, M. O.: Global budget of atmospheric carbonyl
513 sulfide: temporal and spatial variations of the dominant sources and sinks, *J. Geophys. Res.*, 107(D22), 4658,
514 <https://doi.org/10.1029/2002JD002187>, 2002.

515 Kettle, A. J., Rhee, T. S., von Hobe, M., Poulton, A., Aiken, J., and Andreae, M. O.: Assessing the flux of different
516 volatile sulfur gases from the ocean to the atmosphere, *J. Geophys. Res.-Atmos.*, 106(D11), 12193–12209,
517 <https://doi.org/10.1029/2000JD900630>, 2001.

518 Khan, M. A. H., Gillespie, S. M. P., Razis, B., Xiao, P., Davies-Coleman, M. T., Percival, C. J., Derwent, R. G., Dyke,
519 J. M., Ghosh, M. V., Lee, E. P. F., and Shallcross, D. E.: A modelling study of the atmospheric chemistry of DMS
520 using the global model, STOCHEM-CRI, *Atmos. Environ.*, 127, 69–79.

521 <http://dx.doi.org/10.1016/j.atmosenv.2015.12.028>, 2016.

522 Kim, K.-H., and Andreae, M. O.: Carbon disulfide in estuarine, coastal and oceanic environments, *Mar. Chem.*, 40,
523 179–197, [https://doi.org/10.1016/0304-4203\(92\)90022-3](https://doi.org/10.1016/0304-4203(92)90022-3), 1992.

524 Kurian S, Chndrasekhararao A. V., Vidya P. J., Shenoy D. M., Gauns M., Uskaikar, H., and Aparna, S. G.: Role of
525 oceanic fronts in enhancing phytoplankton biomass in the eastern Arabian Sea during an oligotrophic period, *Mar.*
526 *Environ. Res.*, 160, 105023, <https://doi.org/10.1016/j.marenvres.2020.105023>, 2020.

527 Lennartz, S. T., Gauss, M., von Hobe, M., and Marandino, C. A.: Monthly resolved modelled oceanic emissions of
528 carbonyl sulphide and carbon disulphide for the period 2000–2019, *Earth Syst. Sci. Data*, 13, 2095–2110,
529 <https://doi.org/10.5194/essd-13-2095-2021>, 2021.

530 Lennartz, S. T., Marandino, C. A., von Hobe, M., Andreae, M. O., Aranami, K., Atlas, E., Berkelhammer, M.,
531 Bingemer, H., Booge, D., Cutter, G., Cortes, P., Kremser, S., Law, C. S., Marriner, A., Simó R., Quack, B., Uher,
532 G., Xie, H., and Xu, X.: Marine carbonyl sulfide (OCS) and carbon disulfide (CS₂): a compilation of measurements
533 in seawater and the marine boundary layer, *Earth Syst. Sci. Data*, 12, 591–609, [https://doi.org/10.5194/essd-12-](https://doi.org/10.5194/essd-12-591-2020)
534 [591-2020](https://doi.org/10.5194/essd-12-591-2020), 2020.

535 Lennartz, S. T., Marandino, C. A., von Hobe, M., Cortes, P., Quack, B., Simo, R., Booge, D., Pozzer, A., Steinhoff,
536 T., Arevalo-Martinez, D. L., Kloss, C., Bracher, A., Röttgers, R., Atlas, E., and Krüger, K.: Direct oceanic emissions
537 unlikely to account for the missing source of atmospheric carbonyl sulfide, *Atmos. Chem. Phys.*, 17, 385–402,
538 <https://doi.org/10.5194/acp-17-385-2017>, 2017.

539 Li, J.-L., Zhai, X., and Du, L.: Effect of nitrate on the photochemical production of carbonyl sulfide from surface
540 seawater, *Geophys. Res. Lett.*, 49, e2021GL097051, <https://doi.org/10.1029/2021GL097051>, 2022.

541 Liss, P. S., and Slater, P. G.: Flux of gases across the air-sea interface, *Nature*, 247(5438), 181–184,
542 <https://doi.org/10.1038/247181a0>, 1974.

543 Logan, J. A., McElroy, M. B., Wofsy, S. C., and Prather, M. J.: Oxidation of CS₂ and COS: sources for atmospheric
544 SO₂. *Nature* 281, 185–188. <https://doi.org/10.1038/281185a0>, 1979.

545 Maignan, F., Abadie, C., Remaud, M., Kooijmans, L. M. J., Kohonen, K.-M., Commane, R., Wehr, R., Campbell, J.
546 E., Belviso, S., Montzka, S. A., Raoult, N., Seibt, U., Shiga, Y. P., Vuichard, N., Whelan, M. E., and Peylin, P.:
547 Carbonyl sulfide: comparing a mechanistic representation of the vegetation uptake in a land surface model and the

548 leaf relative uptake approach, *Biogeosciences*, 18, 2917–2955, <https://doi.org/10.5194/bg-18-2917-2021>, 2021.

549 Modiri Gharehveran, M., Hain E, Blaney L, and Shah, A. D.: Influence of dissolved organic matter on carbonyl sulfide
550 and carbon disulfide formation from cysteine during sunlight photolysis, *Environ. Sci.: Processes Impacts*, 22,
551 1852–1864, <https://doi.org/10.1039/D0EM00219D>, 2020.

552 Modiri Gharehveran, M., and Shah, A. D.: Influence of dissolved organic matter on carbonyl sulfide and carbon
553 disulfide formation from dimethyl sulfide during sunlight photolysis, *Water Environ. Res.*, 93, 2982–2997,
554 <https://doi.org/10.1002/wer.1650>, 2021.

555 Naik, B. R., Gauns, M., Bepari, K., Uskaikar, H., and Shenoy, D. M.: Variation in phytoplankton community and its
556 implication to dimethylsulphide production at a coastal station off Goa, India, *Mar. Environ. Res.*, 157, 104926,
557 <https://doi.org/10.1016/j.marenvres.2020.104926>, 2020.

558 Nightingale, P. D., Malin, G., Law, C. S., Watson, A. J., Liss, P. S., Liddicoat, M. I., Boutin, J., and Upstill-Goddard,
559 R. C.: In situ evaluation of air-sea gas exchange parameterizations using novel conservative and volatile tracers,
560 *Global Biogeochem. Cy.*, 14(1), 373–387, <https://doi.org/10.1029/1999GB900091>, 2000.

561 O'Brien, J., McParland, E. L., Bramucci, A. R., Ostrowski, M., Siboni, N., Ingleton, T., Brown, M. V., Levine, N. M.,
562 Laverock, B., Petrou, K., and Seymour, J.: The microbiological drivers of temporally dynamic
563 dimethylsulfoniopropionate cycling processes in Australian coastal shelf waters, *Front. Microbiol.*, 13, 894026,
564 <https://doi.org/10.3389/fmicb.2022.894026>, 2022.

565 Parsons, T. R., Maita, Y., and Lalli, C. M.: A manual of chemical and biological methods for seawater analysis, in
566 Fluorometric determination of chlorophylls, edited by: Parsons, T. R., Maita, Y., and Lalli, C. M., Great Britain,
567 CA: Pergamon Press, 107–109, 1984.

568 Reisch, C. R., Stoudemayer, M. J., Varaljay, V. A., Amster, I. J., Moran, M. A., and Whitman, W. B.: Novel pathway
569 for assimilation of dimethylsulphoniopropionate widespread in marine bacteria, *Nature*, 473(7346), 208–211,
570 <https://doi.org/10.1038/nature10078>, 2011.

571 Remaud, M., Chevallier, F., Maignan, F., Belviso, S., Berchet, A., Parouffe, A., Abadie, C., Bacour, C., Lennartz, S.,
572 and Peylin, P.: Plant gross primary production, plant respiration and carbonyl sulfide emissions over the globe
573 inferred by atmospheric inverse modelling, *Atmos. Chem. Phys.*, 22(4), 2525–2552, [https://doi.org/10.5194/acp-](https://doi.org/10.5194/acp-22-2525-2022)
574 [22-2525-2022](https://doi.org/10.5194/acp-22-2525-2022), 2022.

575 Sandalls, F. J., and Penkett, S. A.: Measurements of carbonyl sulphide and carbon disulphide in the atmosphere, *Atmos.*
576 *Environ.*, 11(2), 197–199, [https://doi.org/10.1016/0004-6981\(77\)90227-X](https://doi.org/10.1016/0004-6981(77)90227-X), 1977.

577 Sander, R.: Compilation of Henry's law constants (version 4.0) for water as solvent, *Atmos. Chem. Phys.*, 15, 4399–
578 4981, <https://doi.org/10.5194/acp-15-4399-2015>, 2015.

579 Schäfer, H., Myronova, N., and Boden, R.: Microbial degradation of dimethylsulphide and related C₁-sulphur
580 compounds: organisms and pathways controlling fluxes of sulphur in the biosphere, *J. Exp. Bot.*, 61(2), 315–334,
581 <https://doi.org/10.1093/jxb/erp355>, 2010.

582 Schlitzer, R.: Ocean Data View, odv.awi.de, 2023.

583 Sciare, J., Mihalopoulos, N., and Nguyen, B. C.: Spatial and temporal variability of dissolved sulfur compounds in
584 European estuaries, *Biogeochemistry*, 59(1–2), 121–141, <http://dx.doi.org/10.1023/A:1015539725017>, 2002.

585 Simó, R., Grimalt, J. O., and Albaigés, J.: Dissolved dimethylsulphide, dimethylsulphoniopropionate and
586 dimethylsulphoxide in western Mediterranean waters, *Deep-Sea Res. Pt II*, 44(3-4), 929–950,
587 [https://doi.org/10.1016/S0967-0645\(96\)00099-9](https://doi.org/10.1016/S0967-0645(96)00099-9), 1997.

588 Staubes, R., and Georgii, H.-W.: Biogenic sulfur compounds in seawater and the atmosphere of the Antarctic region,
589 *Tellus B*, 45(2), 127–137, <https://doi.org/10.3402/tellusb.v45i2.15587>, 1993.

590 Tian, X., Hu, M., and Ma, Q.: Determination of volatile sulfur compounds in the atmosphere and surface seawater in
591 Qingdao, *Acta Scien. Circum.*, 25(1), 30–33, (in Chinese with English abstract),
592 <https://doi.org/10.13671/j.hjkxxb.2005.01.005>, 2005.

593 Turner, S. M., Malin, G., Nightingale, P. D., and Liss, P. S.: Seasonal variation of dimethyl sulphide in the North Sea
594 and an assessment of fluxes to the atmosphere, *Mar. Chem.*, 54(3–4), 245–262, [https://doi.org/10.1016/0304-](https://doi.org/10.1016/0304-4203(96)00028-X)
595 [4203\(96\)00028-X](https://doi.org/10.1016/0304-4203(96)00028-X), 1996.

596 Uher, G., and Andreae, M. O.: Photochemical production of carbonyl sulfide in North Sea water: a process study,
597 *Limnol. Oceanogr.*, 42(3), 432–442, <https://doi.org/10.4319/lo.1997.42.3.0432>, 1997.

598 Ulshöfer, V. S., Flöck, O. R., Uher, G., and Andreae, M. O.: Photochemical production and air-sea exchange of
599 carbonyl sulfide in the eastern Mediterranean Sea, *Mar. Chem.*, 53(53), 25–39, [https://doi.org/10.1016/0304-](https://doi.org/10.1016/0304-4203(96)00010-2)
600 [4203\(96\)00010-2](https://doi.org/10.1016/0304-4203(96)00010-2), 1996.

601 Ulshöfer, V. S., Uher, G., and Andreae, M. O.: Evidence for a winter sink of atmospheric carbonyl sulfide in the
602 northeast Atlantic Ocean, *Geophys. Res. Lett.*, 22(19), 2601–2604, <https://doi.org/10.1029/95GL02656>, 1995.

603 Wang, J., Chu, Y.-X., Tian, G., and He, R.: Estimation of sulfur fate and contribution to VSC emissions from lakes
604 during algae decay, *Sci. Total Environ.*, 856, 159193, <http://dx.doi.org/10.1016/j.scitotenv.2022.159193>, 2023.

605 Watts, S. F.: The mass budgets of carbonyl sulfide, dimethyl sulfide, carbon disulfide and hydrogen sulfide, *Atmos.*
606 *Environ.*, 34, pp. 761–779, [https://doi.org/10.1016/S1352-2310\(99\)00342-8](https://doi.org/10.1016/S1352-2310(99)00342-8), 2000.

607 Weiss, P. S., Johnson, J. E., Gammon, R. H., and Bates, T. S.: Reevaluation of the open ocean source of carbonyl
608 sulfide to the atmosphere, *J. Geophys. Res.-Atmos.*, 100(D11), 23083–23092, <https://doi.org/10.1029/95JD01926>,
609 1995.

610 Whelan, M. E., Lennartz, S. T., Gimeno, T. E., Wehr, R., Wohlfahrt, G., Wang, Y., Kooijmans, L. M. J., Hilton, T.
611 W., Belviso, S., Peylin, P., Commane, R., Sun, W., Chen, H., Kuai, L., Mammarella, I., Maseyk, K., Berkelhammer,
612 M., Li, K.-F., Yakir, D., Zumkehr, A., Katayama, Y., Ogée, J., Spielmann, F. M., Kitz, F., Rastogi, B., Kesselmeier,
613 J., Marshall, J., Erkkilä K.-M., Wingate, L., Meredith, L. K., He, W., Bunk, R., Launois, T., Vesala, T., Schmidt,
614 J. A., Fichot, C. G., Seibt, U., Saleska, S., Saltzman, E. S., Montzka, S. A., Berry, J. A., and Campbell, J. E.:
615 Reviews and syntheses: carbonyl sulfide as a multi-scale tracer for carbon and water cycles, *Biogeosciences*, 15,
616 3625–3657, <https://doi.org/10.5194/bg-15-3625-2018>, 2018.

617 Xie, H., Moore, R. M., and Miller, W. L.: Photochemical production of carbon disulphide in seawater, *J. Geophys.*
618 *Res.-Oceans*, 103(C3), 5635–5644, <https://doi.org/10.1029/97JC02885>, 1998.

619 Xu, F., Zhang, H.-H., Yan, S.-B., Sun, M.-X., Wu, J.-W., and Yang, G.-P.: Biogeochemical controls on climatically
620 active gases and atmospheric sulfate aerosols in the western Pacific, *Environ. Res.*, 220, 115211,
621 <https://doi.org/10.1016/j.envres.2023.115211>, 2023.

622 Xu, X., Bingemer, H. G., Georgii, H.-W., Schmidt, U., and Bartell, U.: Measurements of carbonyl sulfide (COS) in
623 surface seawater and marine air, and estimates of the air-sea flux from observations during two Atlantic cruises, *J.*
624 *Geophys. Res.-Atmos.*, 106(D4), 3491–3502, <https://doi.org/10.1029/2000JD900571>, 2001.

625 Yang, G.-P., Jing, W.-W., Kang, Z.-Q., Zhang, H.-H., and Song, G.-S.: Spatial variations of dimethylsulfide and
626 dimethylsulfoniopropionate in the surface microlayer and in the subsurface waters of the South China Sea during
627 springtime, *Mar. Environ. Res.*, 65, 85–97, <https://doi.org/10.1016/j.marenvres.2007.09.002>, 2008.

628 Yang, G.-P., Song, Y.-Z., Zhang, H.-H., Li, C.-X., and Wu, G.-W.: Seasonal variation and biogeochemical cycling of
629 dimethylsulfide (DMS) and dimethylsulfoniopropionate (DMSP) in the Yellow Sea and Bohai Sea, *J. Geophys.*
630 *Res.-Oceans*, 119(12), 8897–8915, <https://doi.org/10.1002/2014JC010373>, 2014.

631 Yang, G.-P., Zhang, S.-H., Zhang, H.-H., Yang, J., and Liu, C.-Y.: Distribution of biogenic sulfur in the Bohai Sea
632 and northern Yellow Sea and its contribution to atmospheric sulfate aerosol in the late fall, *Mar. Chem.*, 169, 23–
633 32, <https://doi.org/10.1016/j.marchem.2014.12.008>, 2015.

634 Yu, J., Zhang, S.-H., Tian, J.-Y., Zhang, Z.-Y., Zhao, L.-J., Xu, R., Yang, G.-P., Lai, J.-G., Wang, X.-D.: Distribution
635 and dimethylsulfoniopropionate degradation of dimethylsulfoniopropionate-consuming bacteria in the Yellow Sea
636 and East China Sea, *J. Geophys. Res.-Oceans*, 126, e2021JC017679, <https://doi.org/10.1029/2021JC017679>, 2021.

637 Yu, J., Sun, M.-X., and Yang, G.-P.: Occurrence and emissions of volatile sulfur compounds in the Changjiang estuary
638 and the adjacent East China Sea, *Mar. Chem.*, 238, 104062, <https://doi.org/10.1016/j.marchem.2021.104062>, 2022.

639 Yu, J., Wang, S., Lai, J.-G., Tian, J.-Y., Zhang, H.-Q., Yang, G.-P., and Chen, R.: The effect of zooplankton on the
640 distributions of dimethyl sulfide and dimethylsulfoniopropionate in the Bohai and Yellow Seas, *J. Geophys. Res.-*
641 *Oceans*, 128, e2022JC019030, <https://doi.org/10.1029/2022JC019030>, 2023.

642 Zepp, R. G., and Andreae, M. O.: Factors affecting the photochemical production of carbonyl sulfide in seawater,
643 *Geophys. Res. Lett.*, 21(25), 2813–2816, <https://doi.org/10.1029/94GL03083>, 1994.

644 Zhang, Y., Tan, D.-D., He, Z., Yu, J., Yang, G.-P.: Dimethylated sulfur, methane and aerobic methane production in
645 the Yellow Sea and Bohai Sea, *J. Geophys. Res.-Oceans*, 128, e2023JC019736,
646 <https://doi.org/10.1029/2023JC019736>, 2023.

647 Zhang, S.-H., Yang, G.-P., Zhang, H.-H., and Yang, J.: Spatial variation of biogenic sulfur in the south Yellow Sea
648 and the East China Sea during summer and its contribution to atmospheric sulfate aerosol, *Sci. Total Environ.*, 488-
649 489, 157–167, <https://doi.org/10.1016/j.scitotenv.2014.04.074>, 2014.

650 Zhao, Y., Schlundt, C., Booge, D., and Bange, H. W.: A decade of dimethyl sulfide (DMS),
651 dimethylsulfoniopropionate (DMSP) and dimethyl sulfoxide (DMSO) measurements in the southwestern Baltic Sea,
652 *Biogeosciences*, 18, 2161–2179, <https://doi.org/10.5194/bg-18-2161-2021>, 2021.

653 Zhu, R., Yang, G.-P., and Zhang, H.-H.: Temporal and spatial distributions of carbonyl sulfide, dimethyl sulfide, and

654 carbon disulfide in seawater and marine atmosphere of the Changjiang Estuary and its adjacent East China Sea,
655 *Limnol. Oceanogr.*, 64, 632–649, <https://doi.org/10.1002/lno.11065>, 2019.

656 Zhu, R., Zhang, H.-H., and Yang, G.-P.: Determination of volatile sulfur compounds in seawater and atmosphere,
657 *Chin. J. Anal. Chem.*, 45(10), 1504–1510, (in Chinese with English abstract), [https://doi.org/10.11895/j.issn.0253-](https://doi.org/10.11895/j.issn.0253-3820.170291)
658 3820.170291, 2017.

659 Zumkehr, A., Hilton, T. W., Whelan, M., Smith, S., Kuai, L., Worden, J., and Campbell, J. E.: Global gridded
660 anthropogenic emissions inventory of carbonyl sulfide, *Atmos. Environ.*, 183, 11–19,
661 <https://doi.org/10.1016/j.atmosenv.2018.03.063>, 2018.

662

663 **Figure captions**

664 **Fig. 1.** Sampling stations in the Yellow Sea and Bohai Sea during (a) spring and (b) summer (▲ indicates stations
665 where atmospheric samples were collected). Yellow Sea Cold Water Mass: YSCWM. The maps were plotted with
666 Ocean Data View (ODV software) (Schlitzer, 2023).

667 **Fig. 2.** Spatial distributions of temperature, salinity, Chl *a*, COS, DMS, CS₂, and DOC in the surface water of the BS
668 and YS in spring.

669 **Fig. 3.** Spatial distributions of temperature, salinity, Chl *a*, COS, DMS, CS₂, and DOC in the surface water of the BS
670 and YS in summer.

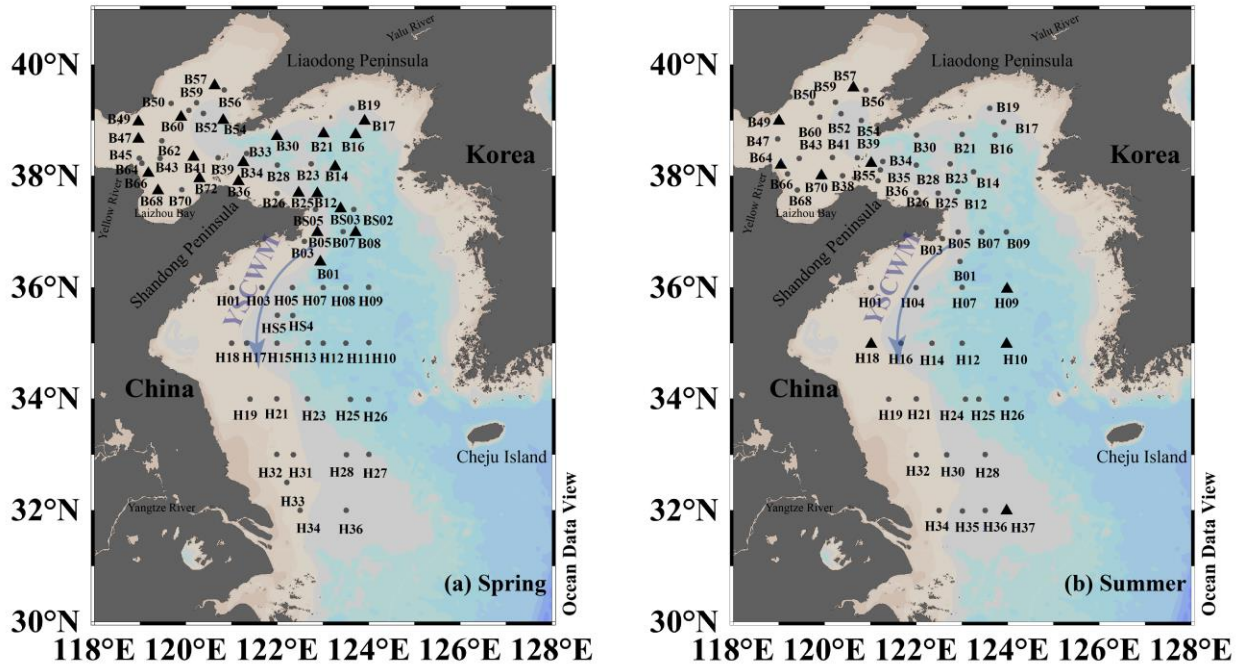
671 **Fig. 4.** Depth distributions of temperature, salinity, Chl *a*, COS, DMS, and CS₂ in seawater in spring.

672 **Fig. 5.** Depth distributions of temperature, salinity, Chl *a*, COS, DMS, and CS₂ in seawater in summer.

673 **Fig. 6.** Spatial distributions of COS, DMS, and CS₂ in the atmosphere over the BS and YS in (a)–(c) spring and (d)–(f)
674 summer. (Unit: pptv)

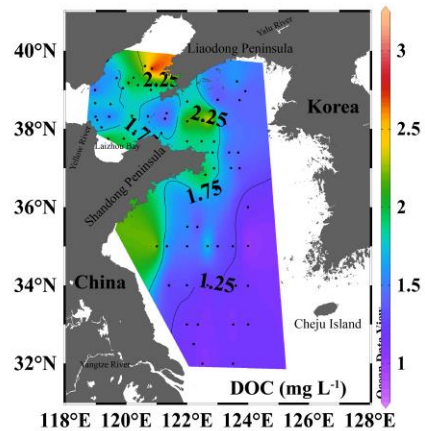
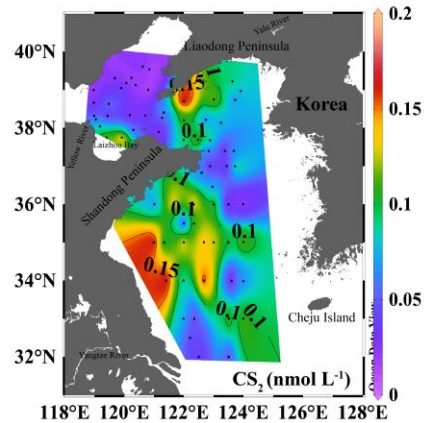
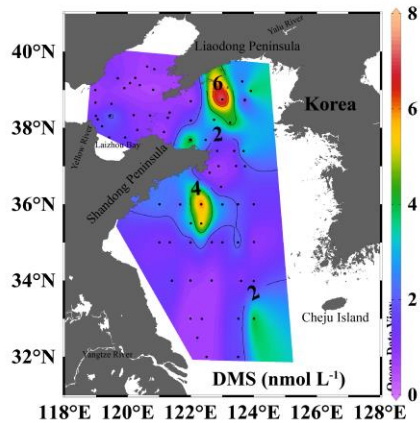
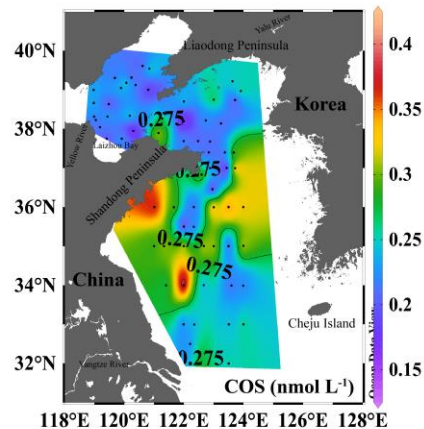
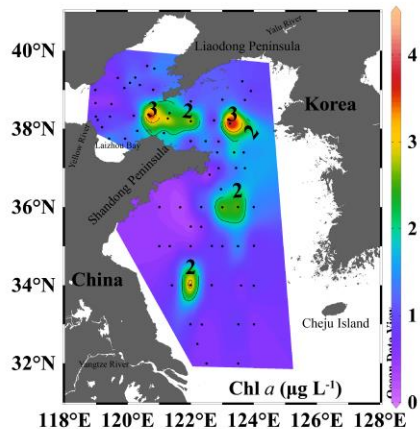
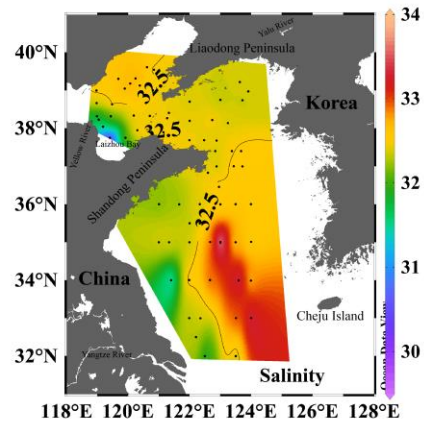
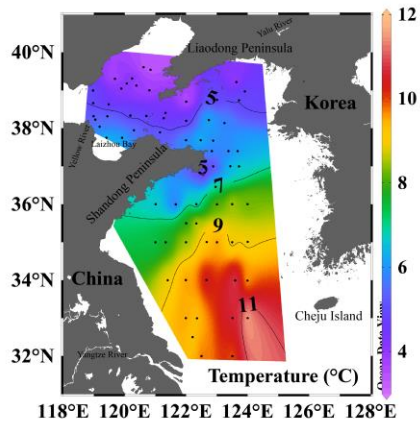
675 **Fig. 7.** Variations in sea-to-air fluxes of VSCs, VSCs concentrations in seawater, and wind speeds in the BS and YS
676 in spring 2018.

677 **Fig. 8.** Variations in sea-to-air fluxes of VSCs, VSCs concentrations in seawater, and wind speeds in the BS and YS
678 in summer 2018.
679

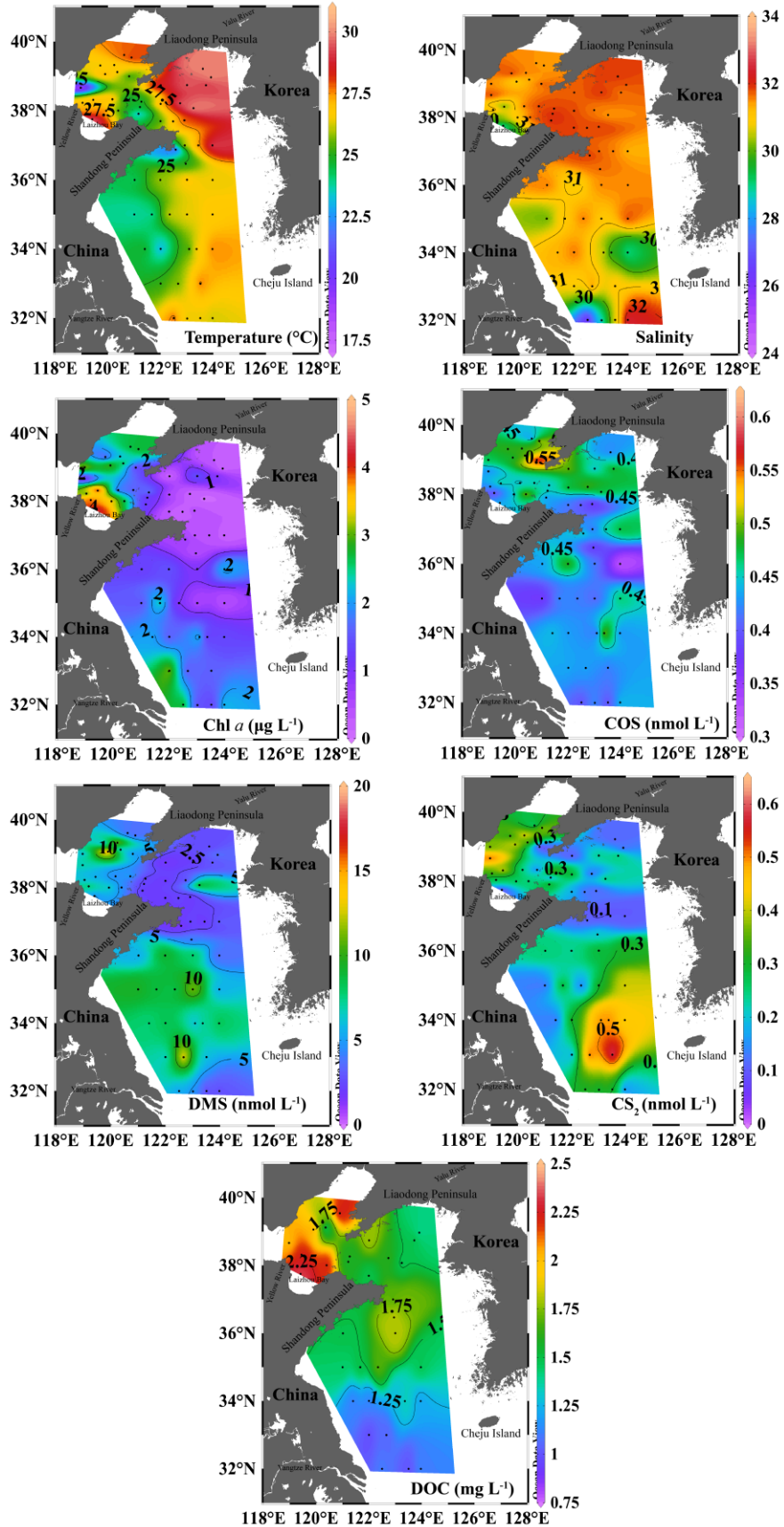


681
682
683
684
685

Fig. 1. Sampling stations in the Yellow Sea and Bohai Sea during (a) spring and (b) summer (▲ indicates stations where atmospheric samples were collected). Yellow Sea Cold Water Mass: YSCWM. The maps were plotted with Ocean Data View (ODV software) (Schlitzer, 2023).



687 **Fig. 2.** Spatial distributions of temperature, salinity, Chl *a*, COS, DMS, CS₂, and DOC in the surface water of the BS
688 and YS in spring.



690 **Fig. 3.** Spatial distributions of temperature, salinity, Chl *a*, COS, DMS, CS₂, and DOC in the surface water of the BS
691 and YS in summer.

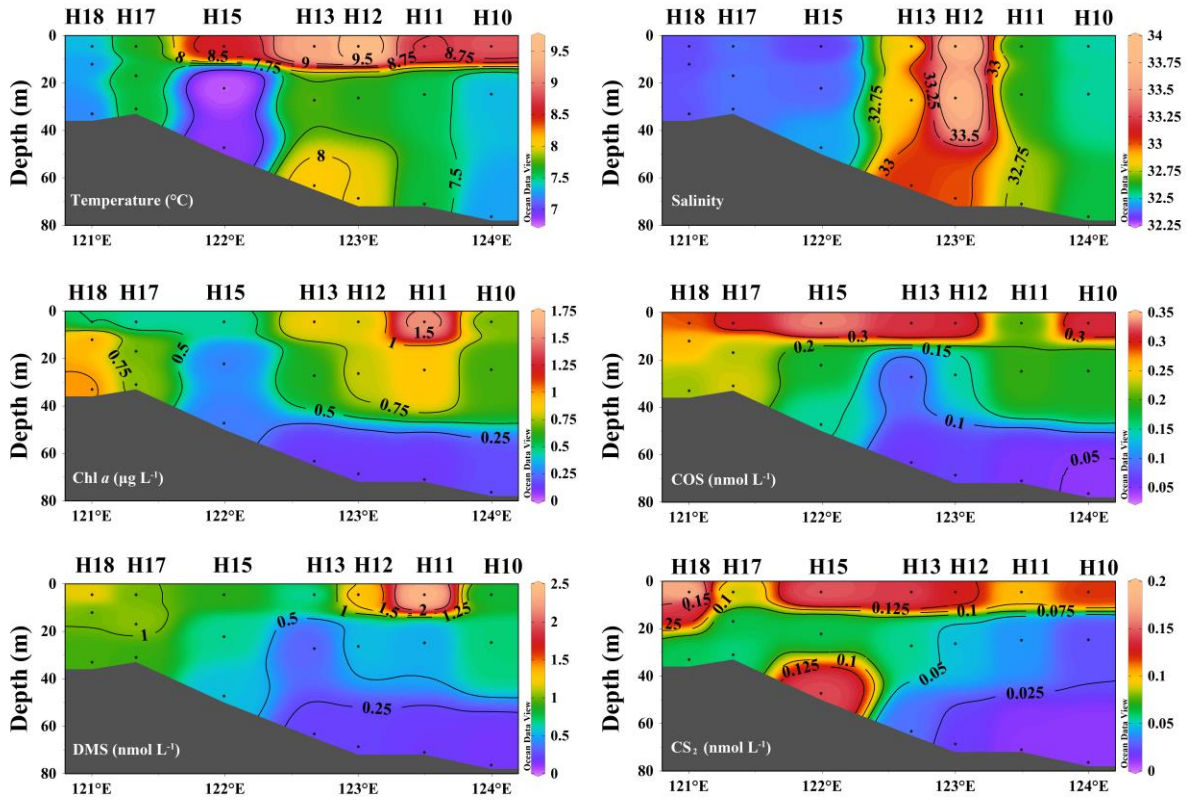
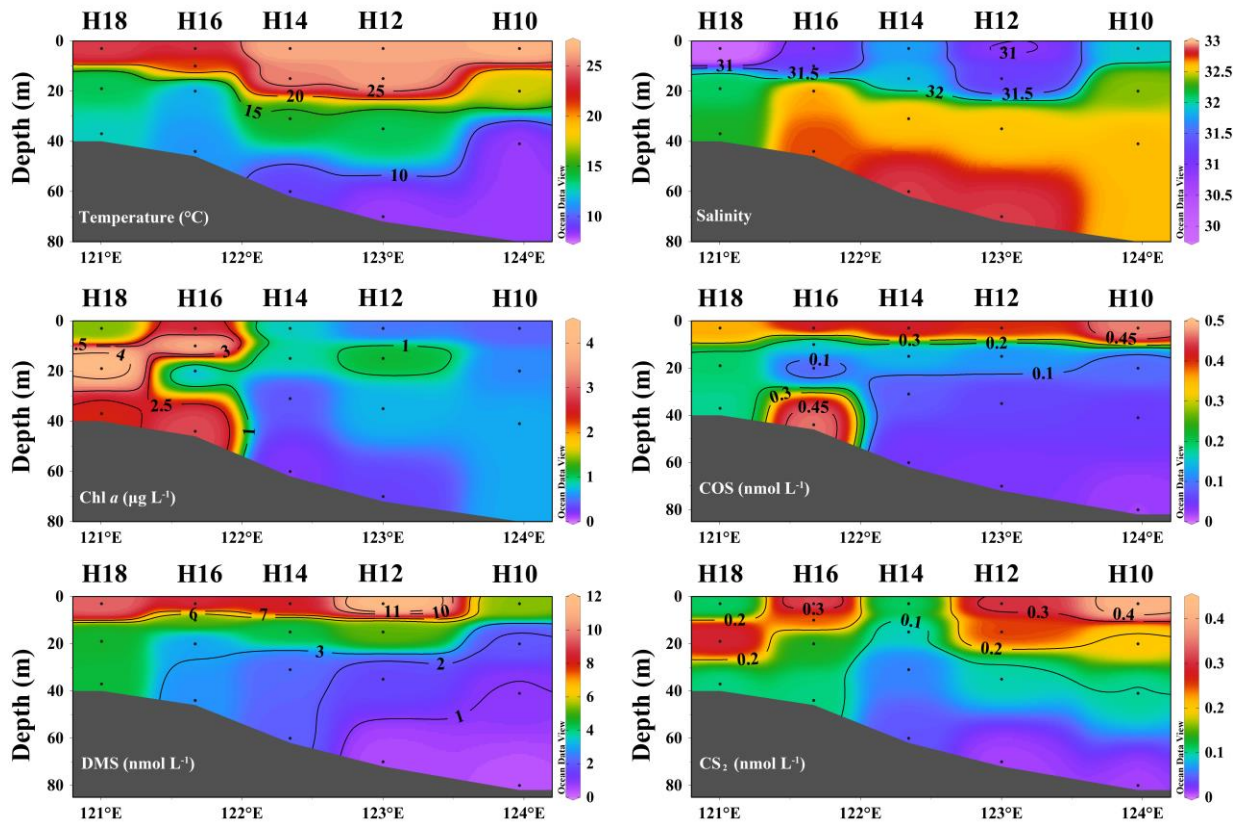


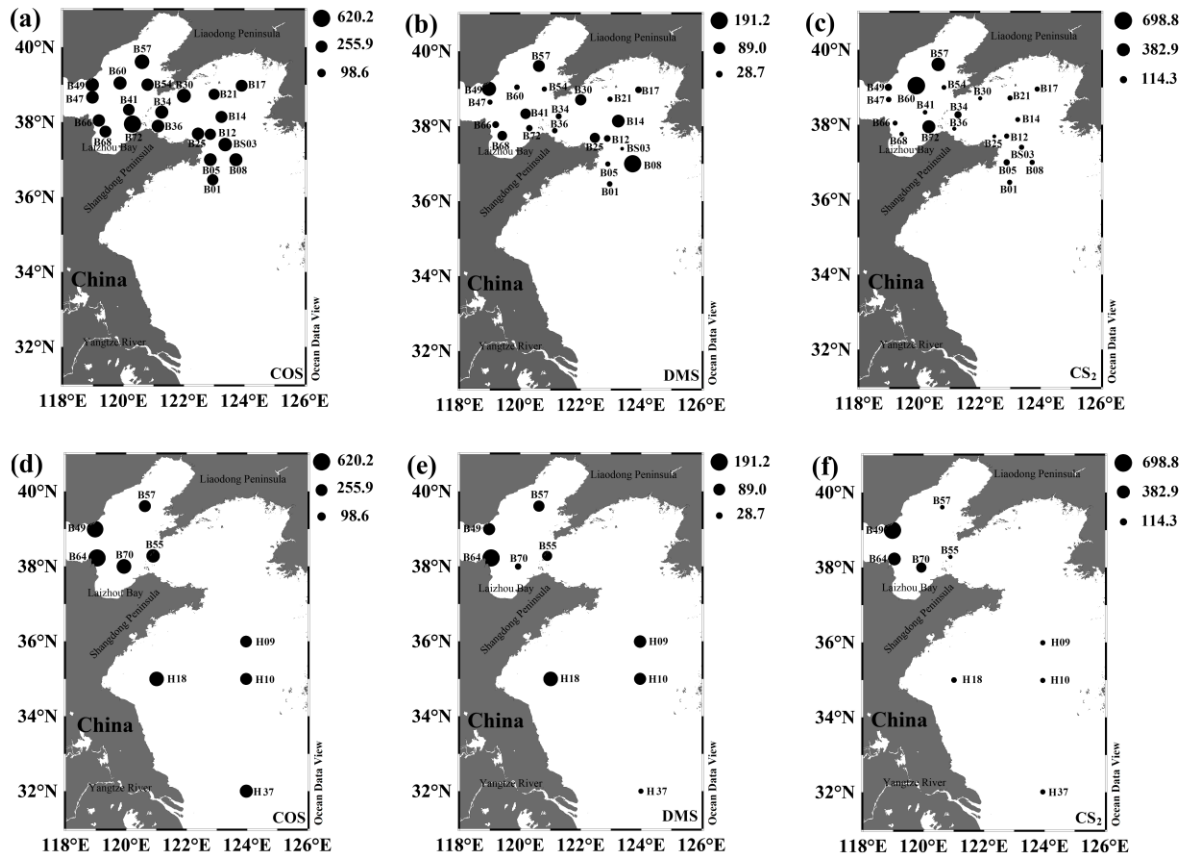
Fig. 4. Depth distributions of temperature, salinity, Chl *a*, COS, DMS, and CS₂ in seawater in spring.

692
693
694



695
696
697

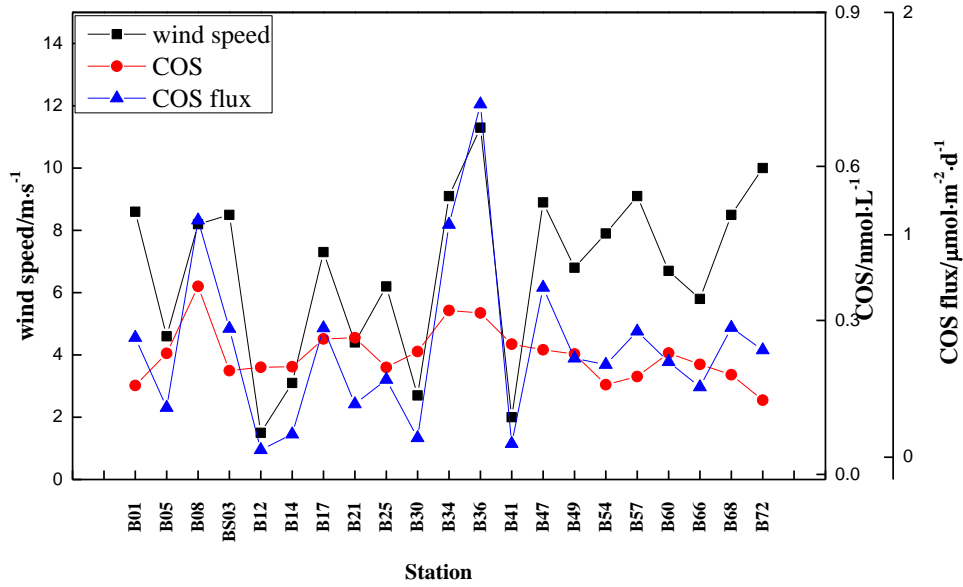
Fig. 5. Depth distributions of temperature, salinity, Chl *a*, COS, DMS, and CS₂ in seawater in summer.



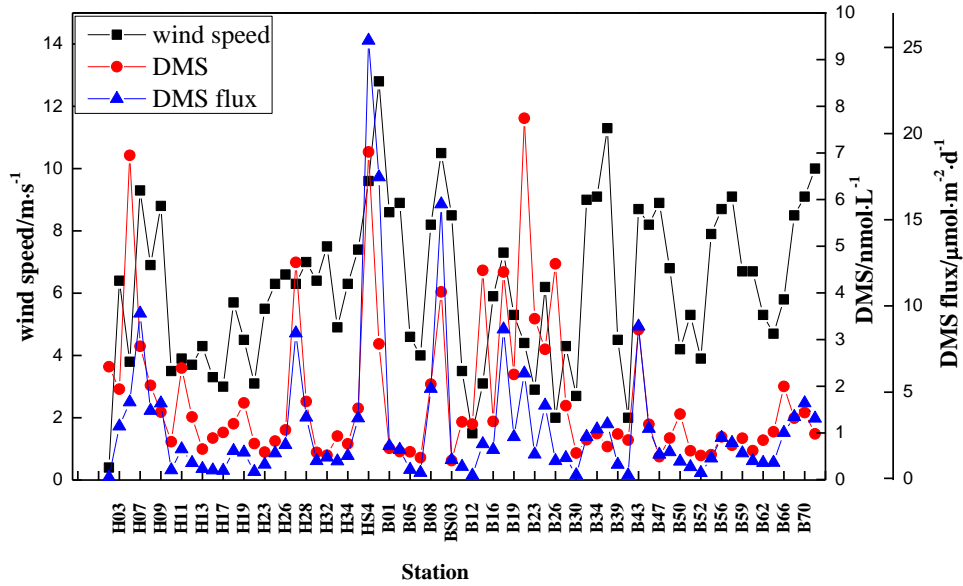
698

699 **Fig. 6.** Spatial distributions of COS, DMS, and CS₂ in the atmosphere over the BS and YS in (a)–(c) spring and (d)–(f)

700 summer. (Unit: pptv)

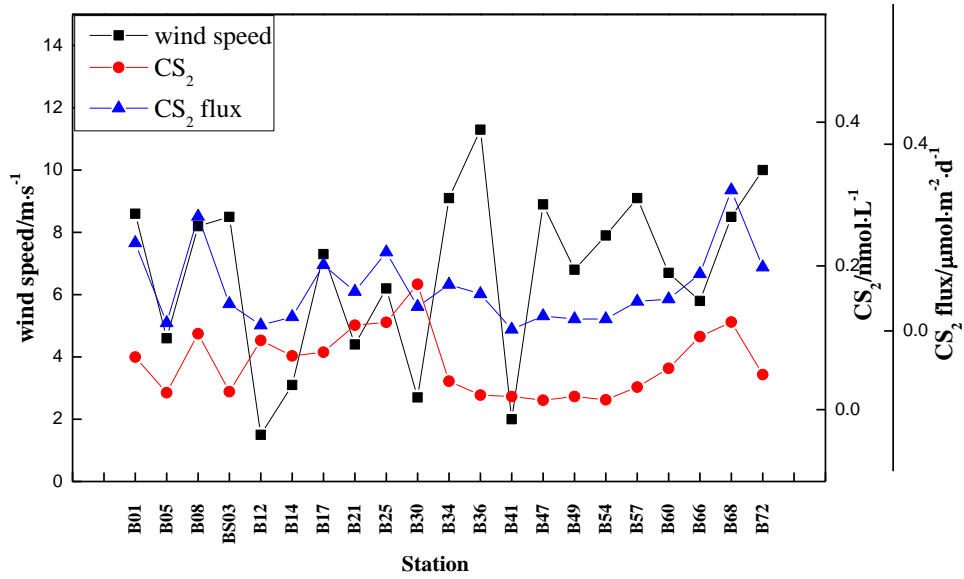


701



702

703

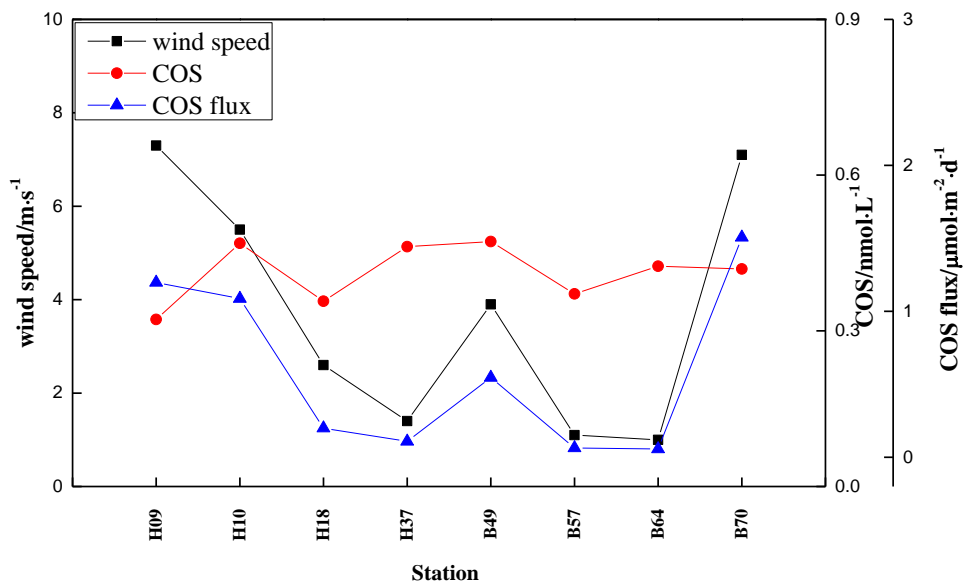


704

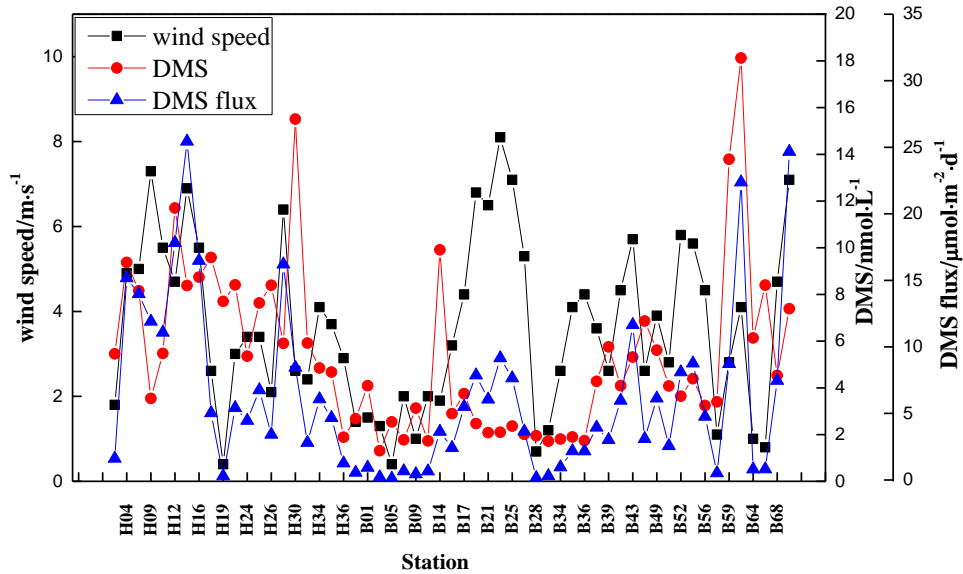
705 **Fig. 7.** Variations in sea-to-air fluxes of VSCs, VSCs concentrations in seawater, and wind speeds in the BS and YS

706

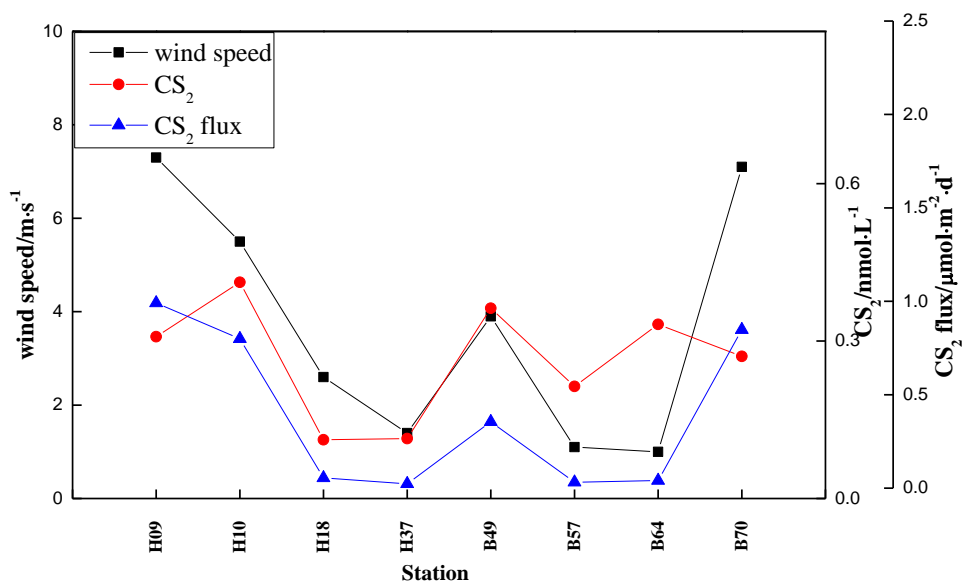
in spring 2018.



707
708



709



710
 711 **Fig. 8.** Variations in sea-to-air fluxes of VSCs, VSCs concentrations in seawater, and wind speeds in the BS and YS
 712 in summer 2018.

713 **Table 1** Correlation analyses of the three VSCs and environmental factors in the BS and YS in spring and summer.

Spring	COS (seawater)	DMS (seawater)	CS ₂ (seawater)	COS (atmosphere)	DMS (atmosphere)	CS ₂ (atmosphere)
COS (seawater)	1					
DMS (seawater)	0.021	1				
CS ₂ (seawater)	0.193	0.281*	1			
COS (atmosphere)	-0.246	-0.355	-0.182	1		
DMS (atmosphere)	0.296	0.04	0.274	0.117	1	
CS ₂ (atmosphere)	-0.201	-0.264	-0.213	0.554**	-0.013	1
Chl <i>a</i>	0.132	0.044	-0.095	0.033	0.179	-0.141
Temperature	0.286*	0.082	0.319**	-0.257	0.179	-0.372
Salinity	0.11	-0.009	-0.109	0.24	0.019	0.236
Silicate	-0.103	-0.252*	-0.029	0.351	-0.008	0.54
Phosphate	-0.084	-0.205	-0.353**	0.621	-0.128	0.36
Nitrate	-0.299*	-0.293*	-0.226	0.075	-0.096	0.044
DOC	-0.146	-0.153	-0.073	0.037	-0.122	0.008
Summer	COS (seawater)	DMS (seawater)	CS ₂ (seawater)	COS (atmosphere)	DMS (atmosphere)	CS ₂ (atmosphere)
COS (seawater)	1					
DMS (seawater)	0.009	1				
CS ₂ (seawater)	-0.007	0.424**	1			
COS (atmosphere)	0.358	0.472	0.184	1		
DMS (atmosphere)	-0.266	0.404	0.31	0.451	1	
CS ₂ (atmosphere)	0.452	0.229	0.424	0.855**	0.251	1
Chl <i>a</i>	-0.059	0.25	0.274*	0.461	-0.294	0.565
Temperature	0.088	-0.076	-0.143	-0.097	-0.349	0.072
Salinity	0.128	-0.172	-0.143	-0.12	-0.352	-0.044
Silicate	0.114	0.122	0.276*	0.312	-0.548	0.377
Phosphate	0.104	-0.169	-0.245	-0.49	-0.539	-0.482
Nitrate	-0.095	0.145	0.057	-0.008	0.224	-0.155
DOC	0.342*	-0.015	0.012	0.02	0.924	0.319

714 * indicates $P < 0.05$, ** indicates $P < 0.01$.